Decuplet baryon structure from lattice QCD

Derek B. Leinweber
Department of Physics and Center for Theoretical Physics, University of Maryland, College Park, Maryland 20742 and TRIUMF, 4004 Wesbrook Mall, Vancouver, British Columbia, Canada V6T 2A3*

Terrence Draper
Department of Physics and Astronomy, University of Kentucky, Lexington, Kentucky 40506

R. M. Woloshyn
TRIUMF, 4004 Wesbrook Mall, Vancouver, British Columbia, Canada V6T 2A3

(Received 9 April 1992)

The electromagnetic properties of the SU(3)-flavor baryon decuplet are examined within a lattice simulation of quenched QCD. Electric charge radii, magnetic moments, and magnetic radii are extracted from the $E0$ and $M1$ form factors. Preliminary results for the $E2$ and $M3$ moments are presented, giving the first model-independent insight to the shape of the quark distribution in the baryon ground state. As in our octet-baryon analysis, the lattice results give evidence of spin-dependent forces and mass effects in the electromagnetic properties. The quark charge distribution radii indicate these effects act in opposing directions. Some baryon dependence of the effective quark magnetic moments is seen. However, this dependence in decuplet baryons is more subtle than that for octet baryons. Of particular interest are the lattice predictions for the magnetic moments of Ω^- and Δ^{++} for which new recent experimental measurements are available. The lattice prediction of the Δ^{++}/p ratio appears larger than the experimental ratio, while the lattice prediction for the Ω^-/p magnetic moment ratio is in good agreement with the experimental ratio.

PACS number(s): 13.40.Fn, 12.38Gc, 14.20.−c

I. INTRODUCTION

Knowledge of the quark substructure of baryons is largely based on experiment and model-dependent descriptions of quark-gluon interactions. While most models are "QCD inspired," they all suffer from an approximate treatment of the complex nonperturbative long distance interactions. Often these interactions are approximated by a simple potential. Quark spin-dependent interactions are approximated by a single gluon or effective pion exchange. In many models the subtleties of current quark and gluon interactions are lumped into an effective or constituent quark mass. Skyrme models offer an alternative description of hadronic phenomena. However, the foundation of the model is in the $1/N_c$ expansion of QCD. To learn the true nature of nonperturbative QCD and, we hope, hadronic phenomena, it is necessary to calculate directly with the QCD Lagrangian in a manner which fully accounts for nonperturbative interactions. The most successful, reliable, and promising approach currently available is that of numerical simulations of QCD.

Through studies of hadronic electromagnetic form factors, the lattice gauge approach to QCD has proven to be a valuable tool in revealing the underlying quark substructure of hadrons [1, 2]. Early calculations focused on the pion electric form factor with SU(2) color [3–5] and later with SU(3) color [6–8]. Calculations of the proton electric form factor followed [9]. Electromagnetic form factors of π, ρ, and N were calculated [2] from which magnetic moments and electric charge radii were extracted. Our analysis of the entire baryon flavor octet followed [1] in which electromagnetic properties were reported for both baryons and the quark sector contributions. This examination of octet baryons exposed the presence of spin-dependent forces and center-of-mass effects in the underlying quark dynamics. These effects give rise to large variations in the quark contributions to baryon magnetic moments which were not anticipated by model calculations. Recently the q^2 dependence of the nucleon electromagnetic form factors was examined using a method which characterizes one of the nucleon interpolating fields as a zero momentum secondary source [10].

Other studies of hadron structure in lattice QCD have been pursued through an examination of current overlap distribution functions [11–13] and Bethe-Salpeter amplitudes [13]. Form factors have a number of advantages over Bethe-Salpeter amplitudes, in that they are gauge invariant, path independent, and allow the extraction of quark distribution radii relative to the system center of mass. In contrast, Bethe-Salpeter amplitudes only give relative quark separations, and subtle dynamical effects can remain hidden.

In this paper we continue our study of hadron structure and present the first lattice QCD calculation of the electromagnetic form factors of SU(3)-flavor-decuplet baryons. An analysis of electromagnetic transition moments will follow in a subsequent paper [14]. The technique for extracting the four form factors associated with

*Present address.

spin-3/2 baryons from the electromagnetic current matrix elements has been outlined in Ref. [15]. From these form factors we will determine magnetic moments, electric radii, and magnetic radii and we will present preliminary results for the higher-order $E2$ and $M3$ moments.

On the lattice, decuplet baryons are stable as a result of the unphysically large quark masses that are used in present calculations. Decay to a pion and an octet baryon is forbidden by energy conservation. However, the stability of decuplet baryons is common to most hadronic models. In this sense, lattice results provide a new forum in which the strengths and weaknesses of various models may be identified. The lattice results also provide access to observables not readily available with present experiments such as the higher-order multipole moments of the Ω^- which is stable to strong interactions.

An examination of decuplet baryon structure in lattice QCD enables one to study new aspects of nonperturbative quark-gluon dynamics. In analyzing the results we make comparisons within the baryon decuplet and with the octet results which provide insight into the spin dependence of quark interactions. The $E2$ and $M3$ moments accessible in spin-3/2 systems provide a preliminary glimpse at the shape of the decuplet baryon ground state. These higher-order moments also have the potential to discriminate between model dependent descriptions of hadronic phenomena. For example, a vanishing $E2$ moment would cast serious doubt on hedgehog Skyrmion descriptions of baryons. To put our results into perspective, we compare our calculations with experimental measurements where available, with recent quark, bag and Skyrme model calculations, and with QCD sum rule calculations.

The format of our paper is as follows. Interpolating fields are discussed in Sec. II A. Correlation functions at the quark level are discussed in Sec. II B. Two-point and three-point correlation functions at the hadronic level are discussed in Secs. II C and II D respectively. Lattice techniques are discussed briefly in Sec. II E. Decuplet baryon masses are reported in Sec. III A. Correlation function ratios used in extracting the multipole form factors are illustrated in Sec. III B. Our findings for the electromagnetic properties of the four multipole form factors are presented in Secs. III C through III F. Finally, Sec. IV provides an overview of our results and a discussion of future investigations.

II. THEORETICAL FORMALISM

A. Interpolating fields

The commonly used interpolating field for exciting the Δ^{++} resonance from the QCD vacuum takes the long established [16, 17] form of

$$\chi_\mu^{\Delta^{++}}(x) = \epsilon^{abc}\left(u^{Ta}(x)C\gamma_\mu u^b(x)\right)u^c(x). \tag{2.1}$$

Unless otherwise noted, we follow the notation of Sakurai [18]. The Dirac gamma matrices are Hermitian and satisfy $\{\gamma_\mu,\gamma_\nu\} = 2\,\delta_{\mu\nu}$, with $\sigma_{\mu\nu} = \frac{1}{2i}[\gamma_\mu,\gamma_\nu]$. $C = \gamma_4\gamma_2$ is the charge conjugation matrix, a, b, c are color indices, $u(x)$ is a u-quark field, and the superscript T denotes a transpose. The generalization of this interpolating field for the Δ^+ composed of two u quarks and one d quark has the form

$$\chi_\mu^{\Delta^+}(x) = \frac{1}{\sqrt{3}}\,\epsilon^{abc}\Big[\,2\,\left(u^{Ta}(x)C\gamma_\mu d^b(x)\right)u^c(x) + \left(u^{Ta}(x)C\gamma_\mu u^b(x)\right)d^c(x)\,\Big]. \tag{2.2}$$

Other decuplet baryon interpolating fields are obtained with the appropriate substitutions of $u(x)$, $d(x) \rightarrow u(x)$, $d(x)$ or $s(x)$. The interpolating field for Σ^{*0} is given by the symmetric generalization

$$\chi_\mu^{\Sigma^{*0}}(x) = \sqrt{\frac{2}{3}}\,\epsilon^{abc}\Big[\,\left(u^{Ta}(x)C\gamma_\mu d^b(x)\right)s^c(x) + \left(d^{Ta}(x)C\gamma_\mu s^b(x)\right)u^c(x) + \left(s^{Ta}(x)C\gamma_\mu u^b(x)\right)d^c(x)\,\Big]. \tag{2.3}$$

The SU(2)-isospin symmetry relationship for Σ^* form factors

$$\Sigma^{*0} = \frac{\Sigma^{*+} + \Sigma^{*-}}{2} \tag{2.4}$$

may be easily seen in the Σ^{*0} interpolating field by noting

$$\epsilon^{abc}\left(s^{Ta}(x)C\gamma_\mu u^b(x)\right)d^c(x) = \epsilon^{abc}\left(u^{Ta}(x)C\gamma_\mu s^b(x)\right)d^c(x). \tag{2.5}$$

B. Correlation functions

Two-point correlation functions at the quark level are obtained through the standard procedure of contracting out pairs of quark fields. Consider the Δ^+ correlation function at the quark level:

$$\left\langle T\left(\chi_\mu^{\Delta^+}(x),\overline{\chi}_\nu^{\Delta^+}(0)\right)\right\rangle = \frac{1}{3}\,\epsilon^{abc}\epsilon^{a'b'c'}\Big\{\,4S_u^{aa'}\,\gamma_\nu\,CS_u^{Tbb'}C\,\gamma_\mu\,S_d^{cc'} + 4S_u^{aa'}\,\gamma_\nu\,CS_d^{Tbb'}C\,\gamma_\mu\,S_u^{cc'} + 4S_d^{aa'}\,\gamma_\nu\,CS_u^{Tbb'}C\,\gamma_\mu\,S_u^{cc'} + 2S_u^{aa'}\,\mathrm{tr}\left[\gamma_\nu\,CS_u^{Tbb'}C\,\gamma_\mu\,S_d^{cc'}\right] + 2S_u^{aa'}\,\mathrm{tr}\left[\gamma_\nu\,CS_d^{Tbb'}C\,\gamma_\mu\,S_u^{cc'}\right] + 2S_d^{aa'}\,\mathrm{tr}\left[\gamma_\nu\,CS_u^{Tbb'}C\,\gamma_\mu\,S_u^{cc'}\right]\Big\}, \tag{2.6}$$

where the quark propagator $S_u^{aa'} = T\left(u^a(x), \overline{u}^{a'}(0)\right)$ and similarly for other quark flavors. SU(3)-flavor symmetry is clearly displayed in this equation.

The corresponding connected three-point function may be constructed by replacing each of the three propagators S, one at a time, by $\widehat{S}$ denoting the propagation of a quark in the presence of the electromagnetic current. The interesting result obtained from (2.6) is that the electromagnetic form factors of the neutral charge decuplet baryons vanish under SU(3)-flavor symmetry. Introduction of the more massive strange quark, as in Σ^{*0} or Ξ^{*0}, violates SU(3)-flavor symmetry and allows a nontrivial result. However, under SU(2)-isospin symmetry the electromagnetic form factors of Δ^0 vanish. A nonzero value for the magnetic moment of the Δ^0 resonance reflects differences in the u- and d-quark masses and contributions from the quark sea through disconnected quark loops interacting with the electromagnetic current.

C. Two-point Green's functions

In this and the following subsection discussing correlation functions at the hadronic level, the Dirac representation of the γ matrices as defined in Itzykson and Zuber [19] is used to facilitate calculations of the γ-matrix algebra. It is then a simple task to account for the differences in γ-matrix and metric definitions in reporting the final results using Sakurai's notation.

The extraction of baryon mass and electromagnetic form factors proceeds through the calculation of the ensemble average (denoted $\langle \cdots \rangle$) of two- and three-point Green's functions. The two-point function is defined as

$$\langle\, G^{BB}_{\sigma\tau}(t;\mathbf{p};\Gamma)\,\rangle = \sum_{\mathbf{x}} e^{-i\mathbf{p}\cdot\mathbf{x}}\Gamma^{\beta\alpha}\,\langle\,\Omega \mid T\left(\chi^{\alpha}_{\sigma}(x)\overline{\chi}^{\beta}_{\tau}(0)\right) \mid \Omega\,\rangle\,. \tag{2.7}$$

Here Ω represents the QCD vacuum, Γ is a 4×4 matrix in Dirac space and α, β are Dirac indices. The subscripts σ, τ are the Lorentz indices of the spin-3/2 interpolating fields. At the hadronic level one proceeds by inserting a complete set of states $\mid B,p,s\,\rangle$ and defining

$$\langle\,\Omega \mid \chi_\sigma(0) \mid B,p,s\,\rangle = Z_B\sqrt{\frac{M}{E_p}}\,u_\sigma(p,s), \tag{2.8}$$

where Z_B represents the coupling strength of $\chi(0)$ to baryon B. The momentum is denoted by p, spin by s, and $u_\alpha(p,s)$ is a spin vector in the Rarita-Schwinger formalism [20]. $E_p = \sqrt{\mathbf{p}^2+M^2}$ and Dirac indices have been suppressed. Using the Rarita-Schwinger spin sum,

$$\sum_s u_\sigma(p,s)\overline{u}_\tau(p,s) = -\frac{\gamma\cdot p + M}{2M}\left\{g_{\sigma\tau} - \frac{1}{3}\gamma_\sigma\gamma_\tau - \frac{2p_\sigma p_\tau}{3M^2} + \frac{p_\sigma\gamma_\tau - p_\tau\gamma_\sigma}{3M}\right\} \equiv \Lambda_{\sigma\tau} \tag{2.9}$$

our usual definitions for Γ,

$$\Gamma_j = \frac{1}{2}\begin{pmatrix}\sigma_j & 0\\ 0 & 0\end{pmatrix}, \quad \Gamma_4 = \frac{1}{2}\begin{pmatrix}I & 0\\ 0 & 0\end{pmatrix}, \tag{2.10}$$

and $\mathbf{p} = (p,0,0)$, the large Euclidean time limit of the two-point function takes the form

$$\langle\, G^{BB}_{\sigma\tau}(t;\mathbf{p},\Gamma_4)\,\rangle = Z_B^2\frac{M}{E_p}e^{-E_p t}\,\mathrm{tr}\left[\,\Gamma_4\,\Lambda_{\sigma\tau}\,\right], \tag{2.11}$$

where

$$\langle\, G^{BB}_{00}(t;\mathbf{p},\Gamma_4)\,\rangle = Z_B^2\frac{2}{3}\frac{|\mathbf{p}|^2}{M_B^2}\left(\frac{E_p+M_B}{2E_p}\right)e^{-E_p t}, \tag{2.12a}$$

$$\langle\, G^{BB}_{11}(t;\mathbf{p},\Gamma_4)\,\rangle = Z_B^2\frac{2}{3}\frac{E_p^2}{M_B^2}\left(\frac{E_p+M_B}{2E_p}\right)e^{-E_p t}, \tag{2.12b}$$

$$\langle\, G^{BB}_{22}(t;\mathbf{p},\Gamma_4)\,\rangle = Z_B^2\frac{2}{3}\left(\frac{E_p+M_B}{2E_p}\right)e^{-E_p t}, \tag{2.12c}$$

$$\langle\, G^{BB}_{33}(t;\mathbf{p},\Gamma_4)\,\rangle = Z_B^2\frac{2}{3}\left(\frac{E_p+M_B}{2E_p}\right)e^{-E_p t}. \tag{2.12d}$$

In determining the appropriate forms suitable for calculations using Sakurai's conventions the definitions of the γ matrices used in the interpolating fields are taken into account. Since the nonvanishing terms of $G^{BB}_{\sigma\tau}$ are diagonal in σ and τ, the γ matrices are paired with their Hermitian conjugates. Since the γ-matrix notation differs only by factors of i and -1, there are no required alterations for calculations using the notation of Sakurai.

Equations (2.12a) through (2.12d) provide four correlation functions from which a baryon mass may be extracted. All baryon masses extracted from the different selections of Lorentz indices agree within statistical uncertainties. The combination providing the smallest statistical fluctuations is $\langle\, G^{BB}_{22}(t;\mathbf{p},\Gamma_4) + G^{BB}_{33}(t;\mathbf{p},\Gamma_4)\,\rangle$ and these results are presented in Sec. III.

It should be noted that the spin-3/2 interpolating field also has overlap with spin-1/2 baryons. For the Δ baryons and Ω^- this poses no problem as these baryons are the lowest-lying baryons in the mass spectrum having the appropriate isospin and strangeness quantum numbers. However, Σ^* and Ξ^* correlation functions may have lower-lying spin-1/2 components and therefore it is desirable to use the spin-3/2 projection operator [21]

$$P^{3/2}_{\mu\nu}(p) = g_{\mu\nu} - \frac{1}{3}\gamma_\mu\gamma_\nu - \frac{1}{3p^2}\left(\gamma\cdot p\,\gamma_\mu p_\nu + p_\mu\gamma_\nu\,\gamma\cdot p\right). \tag{2.13}$$

However, to use this operator, one must calculate the full 4^4 matrix in Dirac and Lorentz spaces of $G^{BB}_{\sigma\tau}(t;\mathbf{p},\Gamma)$ which exceeds our current analysis of four Lorentz terms and two Dirac terms by a factor of 32.

QCD sum rule investigations of Σ^* and Ξ^* hyperons suggest that the spin-1/2 component of the spin-3/2 interpolating field is small relative to the spin-3/2 component [22]. However, the analysis does not determine whether the spin-1/2 component lies above or below the lowest-lying spin-3/2 state. Our lattice results for baryon two-point functions give no indication of a low-lying spin-1/2 component being excited by the spin-3/2 interpolating fields.

D. Three-point functions and multipole form factors

Here we begin with a brief overview of the results of Ref. [15], where the multipole form factors are defined in terms of the covariant vertex functions and in terms of the current matrix elements. The Dirac representation of the γ matrices as defined in Itzykson and Zuber continues to be used to facilitate calculations of the γ-matrix algebra. Finally, the results are reported in Sakurai's notation in a form suitable for calculation in lattice field theory.

The electromagnetic current matrix element for spin-$\frac{3}{2}$ particles may be written as

$$\langle\, p',s' \mid j^\mu(0) \mid p,s \,\rangle = \sqrt{\frac{M_B^2}{E_p E_{p'}}}\,\overline{u}_\alpha(p',s')\mathcal{O}^{\alpha\mu\beta}u_\beta(p,s). \tag{2.14}$$

Here p, p' denote momenta, s , s' spins, and $u_\alpha(p,s)$ is a Rarita-Schwinger spin-vector. The following Lorentz covariant form for the tensor,

$$\mathcal{O}^{\alpha\mu\beta} = -g^{\alpha\beta}\left\{a_1\gamma^\mu + \frac{a_2}{2M_B}P^\mu\right\} - \frac{q^\alpha q^\beta}{(2M_B)^2}\left\{c_1\gamma^\mu + \frac{c_2}{2M_B}P^\mu\right\}, \tag{2.15}$$

where $P = p' + p$, $q = p' - p$ and M_B is the mass of the baryon, satisfies the standard requirements of invariance under time reversal, parity, G parity, and gauge transformations. The parameters a_1, a_2, c_1, and c_2 are independent covariant vertex function coefficients which are related to the multipole form factors.

The multipole expansion of the electromagnetic current matrix element, defined in terms of angular momentum recoupling algebra, has the form

$$\langle\, p',s'|j^0(0)|p,s\,\rangle = A\,\langle\,\frac{3}{2}s' \mid G_{E0}(q^2) + 2\sqrt{5}\tau G_{E2}(q^2)\left[\Sigma^{(2)}\times[\widehat{q}\times\widehat{q}]^{(2)}\right]^{(0)} \mid \frac{3}{2}s\,\rangle, \tag{2.16a}$$

$$\langle\, p',s'|\mathbf{j}(0)|p,s\,\rangle = \sqrt{\tau}\,\langle\,\frac{3}{2}s' \mid \left\{G_{E0}(q^2) + 2\sqrt{5}\tau G_{E2}(q^2)\left[\Sigma^{(2)}\times[\widehat{q}\times\widehat{q}]^{(2)}\right]^{(0)}\right\}\widehat{P} + i\left\{\frac{1}{3}G_{M1}(q^2)\Sigma^{(1)} + 3\tau G_{M3}(q^2)\left[\Sigma^{(3)}\times[\widehat{q}\times\widehat{q}]^{(2)}\right]^{(1)}\right\}\times\widehat{q} \mid \frac{3}{2}s\,\rangle, \tag{2.16b}$$

where $\tau = -q^2/(2M_B)^2$ (≥ 0), and $\widehat{P}$ and $\widehat{q}$ are unit vectors. $A = \sqrt{1+\tau}$ in the laboratory frame ($\mathbf{p} = 0$) and $A = 1$ in the baryon Breit frame ($\mathbf{P} = \mathbf{p}' + \mathbf{p} = 0$). The spin matrix elements are defined by Clebsch-Gordan coefficients:

$$\langle\,\frac{3}{2}s' \mid \frac{3}{2}s\,\rangle = \delta_{s's}, \tag{2.17a}$$

$$\langle\,\frac{3}{2}s' \mid \Sigma^{(1)}_m \mid \frac{3}{2}s\,\rangle = \sqrt{15}\left(\frac{3}{2}s'1m \,\middle|\, \frac{3}{2}1\frac{3}{2}s\right), \tag{2.17b}$$

$$\langle\,\frac{3}{2}s' \mid \Sigma^{(2)}_m \mid \frac{3}{2}s\,\rangle = -\sqrt{\frac{5}{6}}\left(\frac{3}{2}s'2m \,\middle|\, \frac{3}{2}2\frac{3}{2}s\right), \tag{2.17c}$$

$$\langle\,\frac{3}{2}s' \mid \Sigma^{(3)}_m \mid \frac{3}{2}s\,\rangle = -\frac{7}{6}\sqrt{\frac{2}{3}}\left(\frac{3}{2}s'3m \,\middle|\, \frac{3}{2}3\frac{3}{2}s\right), \tag{2.17d}$$

where the Condon and Shortley phase convention has been used [23].

The multipole form factors are defined in terms of the covariant vertex function coefficients a_1, a_2, c_1, and c_2 through the Lorentz-invariant expressions [15]

$$\mathcal{G}_{E0}(q^2) = (1+\tfrac{2}{3}\tau)\{a_1 + (1+\tau)a_2\} - \tfrac{1}{3}\tau(1+\tau)\{c_1 + (1+\tau)c_2\}, \tag{2.18a}$$

$$\mathcal{G}_{E2}(q^2) = \{a_1 + (1+\tau)a_2\} - \tfrac{1}{2}(1+\tau)\{c_1 + (1+\tau)c_2\}, \tag{2.18b}$$

$$\mathcal{G}_{M1}(q^2) = (1+\tfrac{4}{5}\tau)a_1 - \tfrac{2}{5}\tau(1+\tau)c_1, \tag{2.18c}$$

$$\mathcal{G}_{M3}(q^2) = a_1 - \tfrac{1}{2}(1+\tau)c_1. \tag{2.18d}$$

The multipole form factors $\mathcal{G}_{E0}$, $\mathcal{G}_{E2}$, $\mathcal{G}_{M1}$, and $\mathcal{G}_{M3}$ are referred to as charge ($E0$), electric-quadrupole ($E2$), magnetic-dipole ($M1$), and magnetic-octupole ($M3$) multipole form factors, respectively.

In a manner similar to that for the two-point function, the three-point Green function for the electromagnetic current is defined as

$$\langle G_{\sigma\tau}^{Bj^\mu B}(t_2,t_1;\mathbf{p}',\mathbf{p};\Gamma)\rangle = \sum_{\mathbf{x_2},\mathbf{x_1}} e^{-i\mathbf{p}'\cdot\mathbf{x_2}} e^{+i(\mathbf{p}'-\mathbf{p})\cdot\mathbf{x_1}} \Gamma^{\beta\alpha} \langle\Omega|T\left(\chi_\sigma^\alpha(x_2) j^\mu(x_1) \overline{\chi}_\tau^\beta(0)\right)|\Omega\rangle. \tag{2.19}$$

Once again, the subscripts σ, τ are the Lorentz indices of the spin-3/2 interpolating fields. For large Euclidean time separations $t_2 - t_1 \gg 1$ and $t_1 \gg 1$ the three-point function at the hadronic level takes the limit

$$\langle G_{\sigma\tau}^{Bj^\mu B}(t_2,t_1;\mathbf{p}',\mathbf{p};\Gamma)\rangle = \sum_{s,s'} e^{-E_{p'}(t_2-t_1)} e^{-E_p t_1} \Gamma^{\beta\alpha} \langle\Omega|\chi_\sigma^\alpha|p',s'\rangle\langle p',s'|j^\mu|p,s\rangle\langle p,s|\overline{\chi}_\tau^\beta|\Omega\rangle, \tag{2.20}$$

where the matrix element of the electromagnetic current is defined in (2.14), and the matrix elements of the interpolating fields are defined by (2.8).

In Ref. [15] it was noted that the time dependence of the three-point function may be eliminated by use of the two-point functions. However, the appropriate combination of the two-point function Lorentz indices was not specified. Maintaining the lattice Ward identity, which guarantees the lattice electric form factor reproduces the total charge of the baryon at $q^2 = 0$, provides an indispensable guide to the optimum ratio of Green functions. The preferred ratio of two- and three-point Green functions is

$$R_\sigma{}^\mu{}_\tau(t_2,t_1;\mathbf{p}',\mathbf{p};\Gamma) = \left(\frac{\langle\, G_{\sigma\tau}^{Bj^\mu B}(t_2,t_1;\mathbf{p}',\mathbf{p};\Gamma)\,\rangle\langle\, G_{\sigma\tau}^{Bj^\mu B}(t_2,t_1;-\mathbf{p},-\mathbf{p}';\Gamma)\,\rangle}{\langle\, G_{\sigma\tau}^{BB}(t_2;\mathbf{p}';\Gamma_4)\,\rangle\langle\, G_{\sigma\tau}^{BB}(t_2;-\mathbf{p};\Gamma_4)\,\rangle}\right)^{1/2} \tag{2.21}$$

$$\simeq \left(\frac{E_p+M}{2E_p}\right)^{1/2}\left(\frac{E_{p'}+M}{2E_{p'}}\right)^{1/2} \overline{R}_\sigma{}^\mu{}_\tau(\mathbf{p}',\mathbf{p};\Gamma), \tag{2.22}$$

where we have defined the reduced ratio $\overline{R}_\sigma{}^\mu{}_\tau(\mathbf{p}',\mathbf{p};\Gamma)$. Note that there is no implied sum over σ and τ in (2.21).

Using our standard definitions for Γ given in (2.10) and the Rarita-Schwinger spin sum of (2.9), the multipole form factors may be isolated and extracted. The appropriate combinations of $\overline{R}_\sigma{}^\mu{}_\tau(\mathbf{p}',\mathbf{p};\Gamma)$ suitable for calculations employing the γ-matrix and metric conventions of Sakurai are

$$\mathcal{G}_{E0}(q^2) = \frac{1}{3}\left[\overline{R}_1{}^4{}_1(\mathbf{q}_1,0;\Gamma_4) + \overline{R}_2{}^4{}_2(\mathbf{q}_1,0;\Gamma_4) + \overline{R}_3{}^4{}_3(\mathbf{q}_1,0;\Gamma_4)\right], \tag{2.23a}$$

$$\mathcal{G}_{E2}(q^2) = 2\frac{M(E+M)}{|\mathbf{q}_1|^2}\left[\overline{R}_1{}^4{}_1(\mathbf{q}_1,0;\Gamma_4) + \overline{R}_2{}^4{}_2(\mathbf{q}_1,0;\Gamma_4) - 2\overline{R}_3{}^4{}_3(\mathbf{q}_1,0;\Gamma_4)\right], \tag{2.23b}$$

$$\mathcal{G}_{M1}(q^2) = -\frac{3}{5}\frac{E+M}{|\mathbf{q}_1|}\left[\overline{R}_1{}^3{}_1(\mathbf{q}_1,0;\Gamma_2) + \overline{R}_2{}^3{}_2(\mathbf{q}_1,0;\Gamma_2) + \overline{R}_3{}^3{}_3(\mathbf{q}_1,0;\Gamma_2)\right], \tag{2.23c}$$

$$\mathcal{G}_{M3}(q^2) = -4\frac{M(E+M)^2}{|\mathbf{q}_1|^3}\left[\overline{R}_1{}^3{}_1(\mathbf{q}_1,0;\Gamma_2) + \overline{R}_2{}^3{}_2(\mathbf{q}_1,0;\Gamma_2) - \frac{3}{2}\overline{R}_3{}^3{}_3(\mathbf{q}_1,0;\Gamma_2)\right], \tag{2.23d}$$

where $\mathbf{q}_1 = (q,0,0)$. Equation (2.23b) for $\mathcal{G}_{E2}$ isolates the spin matrix element $\langle\ \frac{3}{2}s'\ |\ \Sigma_0^{(2)}\ |\ \frac{3}{2}s\ \rangle$. Smaller statistical uncertainties may be obtained by using the symmetry $\overline{R}_2{}^4{}_2(\mathbf{q}_1,0;\Gamma_4) = \overline{R}_3{}^4{}_3(\mathbf{q}_1,0;\Gamma_4)$. This symmetry is used in the following analysis to eliminate the term $\overline{R}_2{}^4{}_2(\mathbf{q}_1,0;\Gamma_4)$ in the $E2$ form factor. The signs of the $E2$ form factors remain unchanged.

It is worth noting at this point that the form of the tensor $\mathcal{O}^{\alpha\mu\beta}$ in (2.15) is not unique. While equations (2.23a) through (2.23d) are derived using (2.15) these results are more generally applicable. For example, the authors of Ref. [24] employ the form

$$\mathcal{O}^{\alpha\mu\beta} = g^{\alpha\beta}\left\{F_1\gamma^\mu + \frac{F_2}{2M_B}i\sigma^{\mu\nu}q_\nu\right\} + \frac{q^\alpha q^\beta}{2M_B^2}\left\{F_3\gamma^\mu + \frac{F_4}{2M_B}i\sigma^{\mu\nu}q_\nu\right\}. \tag{2.24}$$

Provided one includes a factor of $\sqrt{6}$ to account for their normalization of the $M3$ form factor, the results of (2.23a) through (2.23d) isolate the multipole form factors.

E. Lattice techniques

Here we briefly summarize the lattice techniques used in the following calculations. Additional details may be found in Ref. [1].

We use Wilson's formulation for both the gauge and fermionic action. SU(2)-isospin symmetry is enforced by equating the Wilson hopping parameters $\kappa_u = \kappa_d = \kappa$. We select three values of κ, which we denote $\kappa_1 = 0.152$, $\kappa_2 = 0.154$, and $\kappa_3 = 0.156$, and extrapolate the u-d quark sector to the chiral limit. To account for the relatively heavy strange quark we fix $\kappa_s = \kappa_1$, the smallest of the three values of κ considered. This allows an acceptable extrapolation of the light quarks to the chiral limit through values of quark mass less than or equal to the strange quark mass. Our calculations of octet and decuplet baryon masses indicate that this selection for κ_s gives a reasonable description of the strange quark dynamics.

The conserved electromagnetic current is derived from the fermionic action by the Noether procedure. The lattice Ward identity guarantees the lattice electric form factor reproduces the total baryon charge at $q^2 = 0$.

The quark propagators coupled with fixed momentum $\mathbf{q}_1 = (q,0,0)$ to j^μ are calculated using the sequential source technique (SST) [25–27].

To minimize noise in the Green functions, we exploit the parity symmetry of the correlation functions, and the equal weighting of $\{U\}$ and $\{U^*\}$ gauge configurations in the lattice action. Defining s_P as

$$G(\mathbf{p}',\mathbf{p},\mathbf{q};\Gamma) = s_P\, G(-\mathbf{p}',-\mathbf{p},-\mathbf{q};\Gamma), \qquad s_P = \pm 1, \tag{2.25}$$

and s_C as

$$\Gamma = s_C \left(\widetilde{C}\Gamma\widetilde{C}^{-1}\right)^*, \qquad s_C = \pm 1, \tag{2.26}$$

where $\widetilde{C} = C\gamma_5$, the correlation functions are real provided

$$s_C = s_P. \tag{2.27}$$

This condition is satisfied with the selections for Γ indicated in (2.23a) though (2.23d). While this approach requires an extra matrix inversion to determine an additional SST propagator with momentum $-\mathbf{q}_1$, inclusion of both $\{U\}$ and $\{U^*\}$ configurations in the calculation of the correlation functions provides an unbiased estimate of the ensemble average properties which has substantially reduced fluctuations [28].

Twenty-eight quenched gauge configurations are generated by the Cabibbo-Marinari [29] pseudo-heat-bath method on a $24\times12\times12\times24$ periodic lattice at $\beta = 5.9$. Dirichlet boundary conditions are used for fermions in the time direction. Configurations are selected after 5000 thermalization sweeps from a cold start, and every 1000 sweeps thereafter [30]. Time slices are labeled from 1 to 24, with the δ-function source at $t = 4$. A symmetric combination of the current $[j^\mu(x_1-\widehat{\mu})+j^\mu(x_1)]/2$ is centered at time slice $t_1 = 12$. The following calculations are done in the lab frame $\mathbf{p} = 0$, $\mathbf{p}' = \mathbf{q}_1 = (2\pi/24,0,0)$, the minimum nonzero momentum available on our lattice. The spatial direction of the electromagnetic current is chosen in the z direction. As discussed in Sec. III B and as in Ref. [1], the reported masses and form factors are determined by fitting the correlation functions in time slices 16 through 20 inclusive.

Statistical uncertainties are calculated in a third-order, single elimination jackknife [31, 32]. A third-order jackknife provides uncertainty estimates for the correlation functions, fits to the correlation functions, and quantities extrapolated to the chiral limit.

III. RESULTS

A. Baryon mass

Baryon masses are determined by fitting the Euclidean time evolution of baryon two-point functions at three values of κ with the strange quark fixed at the smallest value of κ. The light u and d quarks are extrapolated to $\kappa_{\rm cr}$ where an extrapolation of the squared pion mass vanishes. The nucleon mass is used to define the lattice spacing $a = 0.128(11)$ fm, $a^{-1} = 1.54(13)$ GeV. Figure 1 displays the masses of the decuplet baryons obtained from the combination of two-point functions $G_{22}^{BB}+G_{33}^{BB}$. Octet-baryon masses are also displayed for reference. Experimental masses [33] are indicated by horizontal lines. With the exception of the N-Δ splitting, the baryon masses are reasonably reproduced. Table I summarizes the lattice baryon masses at the three values of κ considered as well as the extrapolated masses. The momentum transfer is relatively insensitive to the baryon mass. For all baryons, $q^2a^2 = 0.067 \pm 0.001$ with the larger values corresponding to the heavier baryons.

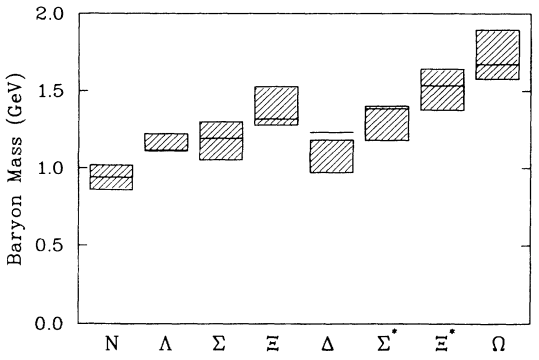

FIG. 1. Octet and decuplet baryon masses. The nucleon mass has been used to set the scale. Horizontal lines indicate the experimental values.

B. Correlation function ratios

Here we present a few of the correlation function ratios of (2.21) which are combined to isolate the multipole form factors. Figure 2 displays the quark contributions to the electric charge form factor of Σ^* hyperons at $\kappa_u = \kappa_3$, the lightest quark masses considered. The d-quark contribution is related to the u-quark result by a ratio of the quark charges. Electric charge form factors for the three charge states of the Σ^* hyperons are obtained through the appropriate sums of quark contributions. Similar results are seen for other decuplet baryons.

The form factors are determined by fitting the correlation function ratio sum by a horizontal line for times

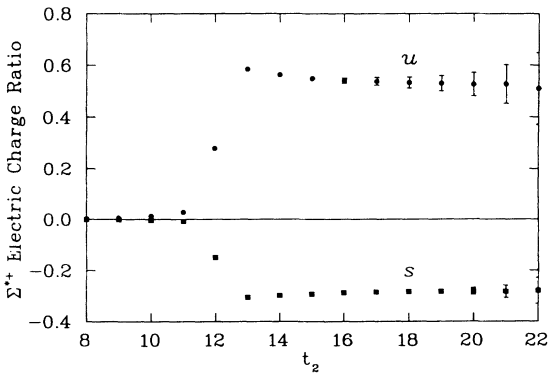

FIG. 2. Quark contributions to the correlation function ratios isolating the Σ^{*+} electric-charge form factor as in (2.23a). The correlation functions are for $\kappa_u = \kappa_3$. Ratios for larger quark mass have smaller statistical uncertainties.

TABLE I. Baryon mass in lattice units ($M_B a$).

Baryon	$\kappa_1 = 0.152$	$\kappa_2 = 0.154$	$\kappa_3 = 0.156$	$\kappa_{cr} = 0.1598(2)$
N	1.09(3)	0.96(3)	0.84(3)	0.61(5)
Δ	1.13(3)	1.02(4)	0.90(5)	0.70(7)
Σ^*	1.13(3)	1.05(4)	0.98(4)	0.84(5)
Ξ^*	1.13(3)	1.09(4)	1.05(4)	0.98(4)
Ω	1.13(3)			1.13(3)

$t_2 >> 12$ and $t_2 << 24$. Fortunately there is a rather broad plateau region where the electric form factor may be reliably determined. We consider fits of the correlation functions from time slice 15 through 21 in intervals including 4 to 7 points. The results are selected from these 10 fits based on the flatness of the correlation functions and the statistical uncertainties. As in the octet baryon analysis, it is found that fits of the 5 points in the time slice interval 16 to 20 provide the optimum balance between these systematic and statistical uncertainties.

Figure 3 shows a similar plot for the quark contributions to the magnetic-dipole form factor of Ξ^* hyperons. Once again $\kappa_u = \kappa_3$ with κ_s fixed at κ_1.

Figures 4 and 5 display the $E2$ and $M3$ ratio sums for Δ baryons in comparison with $E0$ and $M1$ ratio sums respectively. Only the ratio terms appearing inside the square brackets of (2.23a) through (2.23d) are included here. The higher-order moments are dependent upon subtle differences in the ratio contributions, $R_\sigma{}^{\mu}{}_{\tau}$. Fortunately the statistical uncertainties of individual correlation function ratios are correlated and some of the uncertainty is canceled in the higher-order moment sums. However, statistical uncertainties in the $E2$ and $M3$ moments remain large.

The $E2$ result is small relative to the $E0$ ratio sum. In the interest of placing an upper limit on the magnitude of the $E2$ form factor we will consider fits of the $E2$ correlation functions in the standard interval of $t_2 = 16$ through 20. The $M3$ moment is finite and remains finite for all three values of κ considered. This is not entirely surprising as pure $M1$ multipole moments are generally not seen in extended physical systems. Unfortunately, a clear plateau region is not seen. To determine the scale of the $M3$ moment we will fit the correlation function ratio sum in the standard interval of $t_2 = 16$ through 20 with the understanding that the result may be an underestimate of the $M3$ moment.

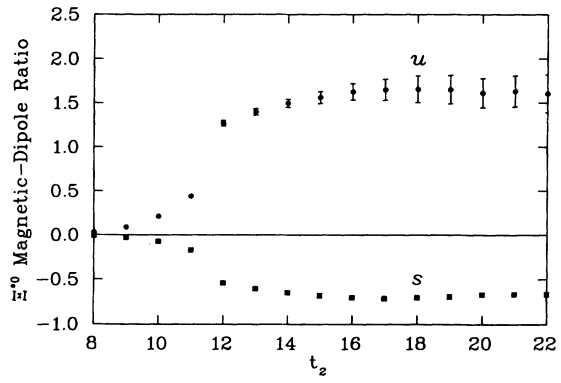

FIG. 3. Quark contributions to the correlation function ratios isolating the Ξ^{*0} magnetic-dipole form factor as in (2.23c). For purposes of illustration the leading kinematical factor, which varies in the second-order jackknife procedure, has been set to a constant. The correlation functions are for $\kappa_u = \kappa_3$. Ratios for larger quark mass have smaller statistical uncertainties.

C. Electric charge form factors

Electric charge form factors are extracted from fits of the ratios in (2.23a). Table II reports the form factors for the decuplet baryons at the three values of κ considered along with the extrapolated values. Table III gives the form factors for individual quarks of unit charge within decuplet baryons. Note that isospin symmetry equates d-quark properties to u-quark properties when normalized to unit charge.

We use the standard small q^2 expansion of the Fourier transform of a spherical charge distribution to extract the electric charge radius.

$$\langle r^2 \rangle = -6\frac{d}{dq^2}\mathcal{G}_E(q^2)\,|_{q^2=0}\,. \tag{3.1}$$

We have two points describing the function $\mathcal{G}_E(q^2)$. Namely $\mathcal{G}_E(0)$, the total charge of the baryon, and $\mathcal{G}_E(q^2)$ evaluated at the smallest finite value of q^2 available on our lattice. To evaluate the derivative of (3.1) we use a dipole form for the function $\mathcal{G}_E(q^2)$. The dipole result

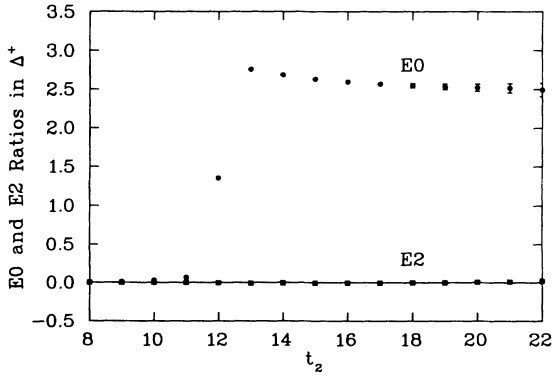

FIG. 4. A comparison of the ratio sums in the square brackets of Eqs. (2.23a) and (2.23b) isolating $\mathcal{G}_{E0}$ and $\mathcal{G}_{E2}$ respectively. Correlation function ratios are for $\kappa_u = \kappa_1$.

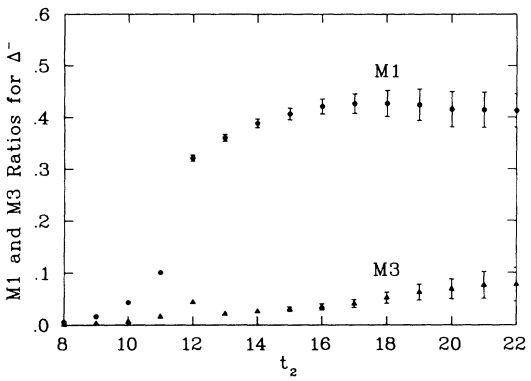

FIG. 5. A comparison of the ratio sums in the square brackets of Eqs. (2.23c) and (2.23d) isolating $\mathcal{G}_{M1}$ and $\mathcal{G}_{M3}$ respectively. The $M3$ form factor is finite. However, the ratio fails to form a clear plateau. Correlation function ratios are for $\kappa_u = \kappa_1$.

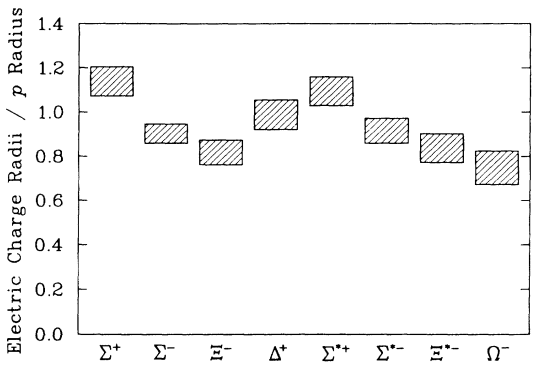

FIG. 6. Electric charge radii for charged octet and decuplet baryons in units of the proton charge radius. Radii of Δ^{++} and Δ^- are equal to that of Δ^+ when normalized by the total baryon charge.

for the radius is

$$\frac{\langle r^2 \rangle}{\mathcal{G}_E(0)} = \frac{12}{q^2}\left(\sqrt{\frac{\mathcal{G}_E(0)}{\mathcal{G}_E(q^2)}} - 1\right). \tag{3.2}$$

To assess the sensitivity of our results on the dipole approximation we also consider a monopole form.

In the figures and tables of this section we quote the quantity $\sqrt{\langle r^2 \rangle}/\mathcal{G}_E(0)$ which gives the radius of baryons and quark distributions with unit charge. In all cases the sign of $\langle r^2 \rangle$ is the same as the charge of the baryon or quark. The difference of the radii extracted in the dipole and monopole approximations is small relative to the statistical uncertainties in the radii. We refer to the dipole results in the following discussion and figures.

The charge radii of decuplet baryons are not determined by experiment so our goal here is to compare decuplet and octet results to see if there is some indication of how spin-dependent interactions affect the electromagnetic structure. Of course the spin-dependent interactions depend on the quark masses and our calculations are done at masses which are not yet small. However the extrapolation of charge radii into the physical (light) quark region is problematic since charge radii become infinite in the exact chiral limit [34]. To reproduce this behavior in the present calculation would require some model-dependent theoretical input which is not available.

To estimate the charge radii in the physical mass region and allow a comparison with model calculations which often neglect couplings to the continuum, we extrapolate in $1/\kappa$ (or equivalently in m_π^2) to $\kappa_{\rm cr}$. Although this prescription involves some systematic uncertainty [35], it gives a better picture of what is happening at physical quark masses than, for example, using only results calculated at our largest κ value. However it should be noted that the qualitative statements and conclusions are the same whether we extrapolate or not.

Figure 6 displays the lattice results for the electric charge radii normalized to the proton charge radius for the charged members of the baryon octet and decuplet. We find a similar pattern of quark mass effects in the octet and decuplet with a Δ^+ charge radius essentially equal to that of the proton. Note that the charge radii of Δ^{++} and Δ^- are equal to that of Δ^+ when the radii are normalized by the total charge. Table IV summarizes the lattice calculations.

Some insight into quark dynamics may be obtained by examining the behavior of the quark distribution radii in hyperons as the u and d quarks become lighter. Consider for example, the distribution radii of u and s quarks within Σ^+ as the u quarks are extrapolated to $\kappa_{\rm cr}$. Figures 7 and 8 display the quark distribution radii in lattice

TABLE II. Baryon electric charge form factors.

Baryon	$\kappa_1 = 0.152$	$\kappa_2 = 0.154$	$\kappa_3 = 0.156$	$\kappa_{\rm cr} = 0.159\,8(2)$
Δ^{++}	1.723(17)	1.681(27)	1.636(55)	1.562(80)
Δ^+	0.861(9)	0.841(13)	0.818(27)	0.781(40)
Δ^0	0.000	0.000	0.000	0.000
Δ^-	−0.861(9)	−0.841(13)	−0.818(27)	−0.781(40)
Σ^{*+}	0.861(9)	0.831(13)	0.796(28)	0.743(40)
Σ^{*0}	0.000	−0.008(1)	−0.017(5)	−0.032(8)
Σ^{*-}	−0.861(9)	−0.847(11)	−0.831(19)	−0.805(28)
Ξ^{*0}	0.000	−0.016(3)	−0.036(8)	−0.065(14)
Ξ^{*-}	−0.861(9)	−0.854(10)	−0.846(12)	−0.832(16)
Ω^-	−0.861(9)			−0.861(9)

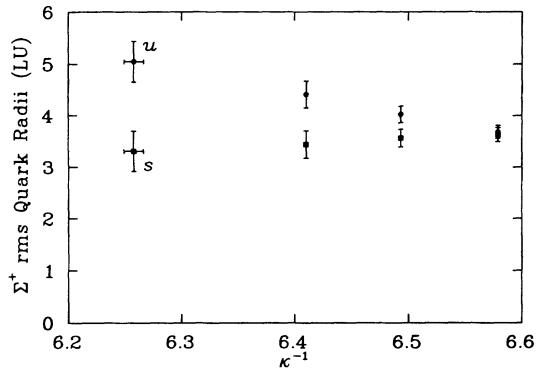

FIG. 7. Extrapolations of the electric charge distributions of quarks within the octet Σ^+ baryon. The radius of the s-quark distribution decreases as the u quarks become lighter.

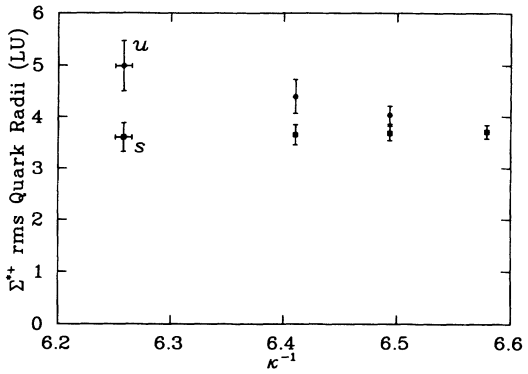

FIG. 8. Extrapolations of the electric charge distributions of quarks within the decuplet Σ^{*+} baryon. The radius of the s-quark distribution is largely unaffected by changes in the u-quark mass.

units (LU) for the octet Σ^+ and the decuplet Σ^{*+} respectively.

In both cases, the radius of the u-quark distribution increases as the u quark becomes lighter (smaller κ^{-1}), as expected. However there is a difference in the behavior of the s-quark distributions in the octet Σ^+ and the decuplet Σ^{*+}. In the case of octet Σ^+, there is a small, but significant, trend for the s-quark distribution radius to decrease as the u quarks become lighter [36]. This effect was understood as a shifting of the center of mass of the u-s system towards the strange quark which becomes relatively heavier as the u quarks become lighter. In contrast, the s-quark distribution radius in the decuplet Σ^{*+} has little dependence on the u-quark mass.

This difference between octet and decuplet behavior has a natural explanation in the hyperfine interaction term of the one-gluon-exchange potential. The hyperfine force is repulsive for quarks interacting in spin-triplet states. The strength of the interaction increases with decreasing u quark mass and provides a mechanism to counteract the center-of-mass effect.

Lattice results for the neutron electric form factor confirm a repulsive force between quarks with their spins aligned. Furthermore, the magnetic form factors indicate that in the octet Σ^+ (decuplet Σ^{*+}), the singly represented s quark has, on average, its spin antialigned (aligned) with that of the doubly represented u quarks. Hence the spin alignments of u and s quarks seen in the lattice results are in qualitative agreement with those anticipated from SU(6)-spin-flavor symmetry. Note however, the lattice dynamics do not impose this symmetry. The quark contributions to octet baryon magnetic moments differ significantly from the SU(6) predictions.

Figure 9 shows charge distribution radii for quarks of unit charge in decuplet baryons. The analogous graph for octet baryons is indicated in Fig. 10. It should be noted that although the uncertainty regions of the radii for different quarks overlap it does not necessarily mean that the u-quark distribution radius in n, for example, may be larger than the u-quark radius in Ξ^0. The uncertainties are highly correlated between the two results and a calculation of the difference of the radii indicates u_Ξ is larger by $0.50^{+0.65}_{-0.15}$ LU. Other octet baryon quark pairs such as $u_\Sigma - u_p$ differ from zero by at least one standard deviation. In the octet, therefore, some nontrivial baryon dependence of the quark distributions does occur. In contrast, significant baryon dependence of the quark distributions in decuplet baryons is not observed. The lattice results are summarized in Table V.

Figure 11 displays ratios of octet and decuplet quark charge distribution radii. With the exception of the singly represented octet quarks u_n and s_Σ which showed some baryon dependence in their charge distributions, the remaining quark distribution radii are unaffected by differences between octet and decuplet spin-flavor symmetry.

Figure 11 also gives an understanding as to why the proton and Δ^+ have similar charge radii. Naively one might expect Δ^+ to be larger due to additional spin-dependent repulsion between the quarks. However, the

TABLE III. Electric charge form factors for single quarks of unit charge.

Quark	$\kappa_1 = 0.152$	$\kappa_2 = 0.154$	$\kappa_3 = 0.156$	$\kappa_{cr} = 0.1598(2)$
u_Δ	0.861(9)	0.841(13)	0.818(27)	0.781(40)
u_{Σ^*}	0.861(9)	0.839(12)	0.814(24)	0.774(34)
s_{Σ^*}	0.861(9)	0.863(9)	0.866(13)	0.869(18)
u_{Ξ^*}	0.861(9)	0.838(12)	0.810(19)	0.767(27)
s_{Ξ^*}	0.861(9)	0.862(9)	0.863(9)	0.865(11)
s_Ω	0.861(9)			0.861(9)

TABLE IV. Baryon rms charge radii normalized to unit charge in lattice units $\langle r^2/a^2 \rangle^{1/2}$.

Baryon	$\kappa_1 = 0.152$	$\kappa_2 = 0.154$	$\kappa_3 = 0.156$	$\kappa_{cr} = 0.1598(2)$
Δ^{++}	3.71(13)	4.02(19)	4.34(39)	4.90(57)
Δ^{+}	3.71(13)	4.02(19)	4.34(39)	4.90(57)
Δ^{-}	3.71(13)	4.02(19)	4.34(39)	4.90(57)
Σ^{*+}	3.71(13)	4.15(19)	4.63(38)	5.42(56)
Σ^{*-}	3.71(13)	3.92(16)	4.16(28)	4.54(41)
Ξ^{*-}	3.71(13)	3.81(14)	3.94(18)	4.15(23)
Ω^{-}	3.71(13)			3.71(13)

dominant effect of the additional spin repulsion is to enhance the charge distribution radius of the d quark in Δ^+ relative to that in p. This counteracts any possible enhancement of u-quark radii in Δ^+.

Some attention has been given to model calculations of the Ω^- charge radius. The model predictions vary over a wide range. Figure 12 illustrates results for the Ω^-/p charge radius ratio. The results include the lattice (Latt) results of this analysis, a calculation based on the relativized quark model (QM) of Ref. [37], MIT bag (MIT) and cloudy bag (CB) models [38], and a bound state approach Skyrme (Skyr) model calculation [39]. Only the relativized quark model calculation agrees with the lattice results.

The electric form factors calculated at $q \simeq 0.4$ GeV for neutral decuplet baryons are illustrated in Fig. 13. Neutral octet baryons are also given for reference. For the hyperons the form factors are dominated by the net charge of the light quarks. Octet and decuplet hyperons display similar behavior. For Δ^0 the symmetric spin state of the quarks causes the form factor to vanish. This contrasts the neutron where the octet-spin asymmetry of the three quarks gives rise to a negative squared charge radius.

With knowledge of quark distribution radii, the charge radii of neutral baryons may be calculated as in $r^2 = \sum_{i=s,s,u} e_i r_i^2$ for Ξ^0. Table VI summarizes the results. The lattice result for the squared charge radius of the neutron $r_n^2/r_p^2 = -0.11^{+0.10}_{-0.14}$ encompasses the experimental value [40, 41] of $-0.167(7)$.

D. Magnetic-dipole form factors

Our calculation of magnetic-dipole form factors is done at the smallest finite value of q^2 available on our lattice. Table VII summarizes the form factors in units of natural magnetons $(e/2M_B)$ where the mass of the baryon appears in the definition of the magneton. The magnetic moment μ is defined at $q^2 = 0$ as $\mathcal{G}_{M1}(0) = \mu/(e/2M_B)$ and therefore we must scale our results from $\mathcal{G}_{M1}(q^2)$ to $\mathcal{G}_{M1}(0)$. Lattice extrapolations in q^2 to $q^2 = 0$ suffer from large statistical errors. To make contact with the experimental magnetic moments, we assume equal scaling of electric and magnetic form factors as in the octet baryon analysis and as supported by experimental measurements of nucleon form factors. In hyperons, the strange and light quark sectors are scaled separately by

$$\frac{\mathcal{G}^s_{M1}(0)}{\mathcal{G}^s_{M1}(q^2)} = \frac{\mathcal{G}^s_E(0)}{\mathcal{G}^s_E(q^2)}, \tag{3.3}$$

and similarly for the light quarks, such that the magnetic moment of a hyperon is given by

$$\mathcal{G}^B_{M1}(0) = \mathcal{G}^l_{M1}(0) + \mathcal{G}^s_{M1}(0), \tag{3.4}$$

where l labels the light quarks. For Δ baryons it is not

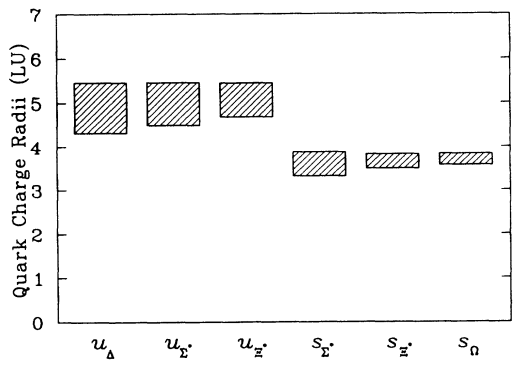

FIG. 9. Charge distribution radii of unit charge quarks within decuplet baryons. Symmetric isospin symmetry equates u- and d-quark properties in decuplet baryons. No significant baryon dependence of the charge radii is seen.

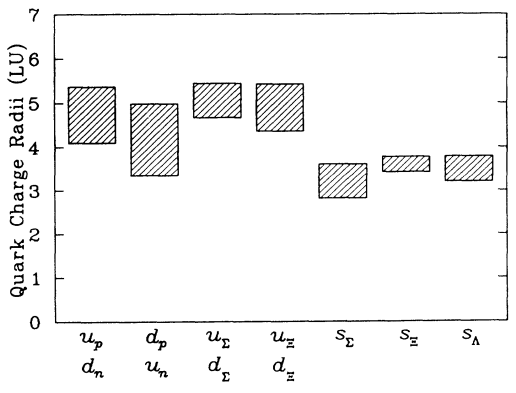

FIG. 10. Charge distribution radii of unit charge quarks within octet baryons. Center-of-mass shifts and spin-dependent forces give rise to significant baryon dependence of the charge radii.

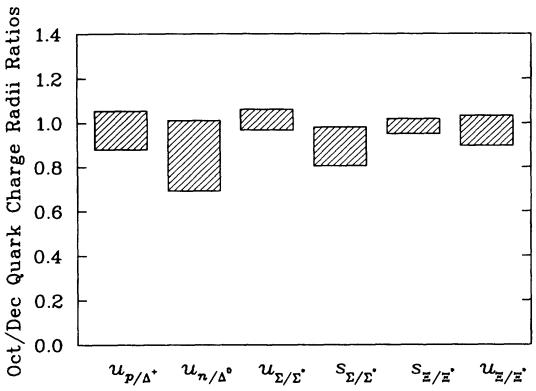

FIG. 11. Ratios of octet and decuplet quark charge distribution radii. Doubly represented quarks show little octet/decuplet baryon dependence.

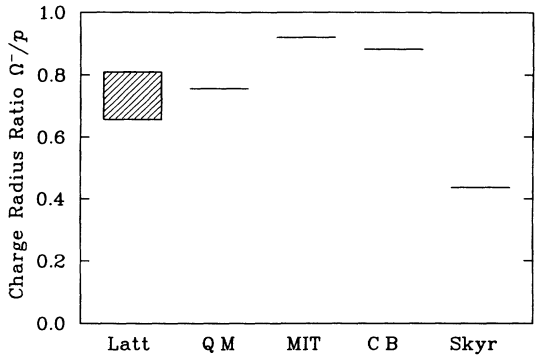

FIG. 12. The Ω^-/p charge radius ratio. The model results include a calculation based on a relativized quark model (QM), MIT bag (MIT) and cloudy bag (CB) models, and a bound state approach Skyrme (Skyr) model. References may be found in the text.

necessary to separate the u- and d-quark sectors due to the SU(2)-isospin symmetry of the correlation functions. Table VIII gives the magnetic-dipole form factors for quarks of unit charge in units of natural magnetons. Combined with the results of Table III the magnetic moments may be calculated.

In the octet baryon analysis it was found that the magnitudes of the lattice results for magnetic moments were consistently smaller than the experimental measurements. It was argued that at $\beta = 5.9$ some deviations from asymptotic scaling may occur. A recent analysis [10] determines nucleon form factors at $\beta = 6.0$ on a cubic lattice with physical spatial dimensions roughly equal to our smaller y and z dimensions. Some improvement is seen in the magnitudes of the magnetic moments which are still 10–15 % low compared with experiment. Chiral dressings of the nucleon may cause our linear extrapolation of the magnetic moments in $1/\kappa$ to underestimate the magnetic moments in the physical regime. Finite volume effects may also give rise to the underestimation of the magnetic moments as the baryon is restricted by its periodic images. The proton rms electric charge radius at κ_3 indicates the proton largely fills the lattice in our smaller y and z spatial dimensions. Nonquenched corrections may also provide additional contributions [42].

To reduce the effects of these uncertainties, ratios of the lattice results to the lattice proton result are used when making comparisons with experimental measurements or model calculations. Table IX reports the extrapolated decuplet baryon magnetic moments in units of nuclear magnetons (μ_N), ratios of decuplet baryon moments, and the proton magnetic moment and ratios scaled to reproduce the proton magnetic moment. These scaled ratios are illustrated in Fig. 14. The expected qualitative behavior of mass dependence is displayed here. For example, as d quarks are replaced by s quarks in going from Δ^- to Σ^{*-} through to Ω^-, the magnetic moments of the negatively charged hyperons decrease in magnitude. As in the case of the electric charge form factors of neutral baryons, the magnetic moments are dominated by the net charges of the light quarks. SU(2)-isospin symmetry causes the Δ^0 moment to vanish.

The simple quark model formula for the magnetic moment of a decuplet baryon is simply given by the sum of the intrinsic moments of the quarks composing the baryon. Results using intrinsic moments determined by the p, n, and Λ moments [33] are also indicated in Fig. 14 by horizontal dashed lines. The agreement is striking and suggests a baryon independence of the lattice effective quark moments.

Figure 15 displays the lattice effective quark moments for quarks of unit charge within decuplet baryons. Effective moments have been defined by equating the lattice quark sector contributions to the same sector of the SU(6)-magnetic-moment formula derived from SU(6)-spin-flavor symmetry wave functions. For example, SU(6)-spin-flavor symmetry gives the simple quark model formula

$$\mu_p = A\mu_u - B\mu_d, \tag{3.5}$$

TABLE V. rms charge radii for single quarks of unit charge in lattice units $\langle\, r^2/a^2 \,\rangle^{1/2}$.

Quark	$\kappa_1 = 0.152$	$\kappa_2 = 0.154$	$\kappa_3 = 0.156$	$\kappa_{cr} = 0.1598(2)$
u_Δ	3.71(13)	4.02(19)	4.34(39)	4.90(57)
u_{Σ^*}	3.71(13)	4.03(18)	4.40(33)	4.99(48)
s_{Σ^*}	3.71(13)	3.68(14)	3.65(20)	3.60(28)
u_{Ξ^*}	3.71(13)	4.05(17)	4.44(27)	5.07(38)
s_{Ξ^*}	3.71(13)	3.70(13)	3.68(14)	3.66(16)
s_Ω	3.71(13)			3.71(13)

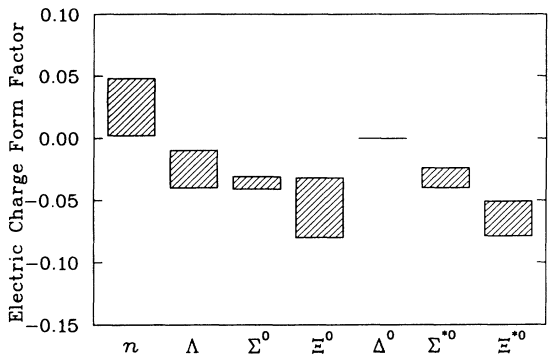

FIG. 13. Electric charge form factors of neutral baryons calculated at $q \simeq 0.4$ GeV. The light quark charges dominate the hyperon form factors while decuplet spin symmetry causes the Δ^0 form factor to vanish.

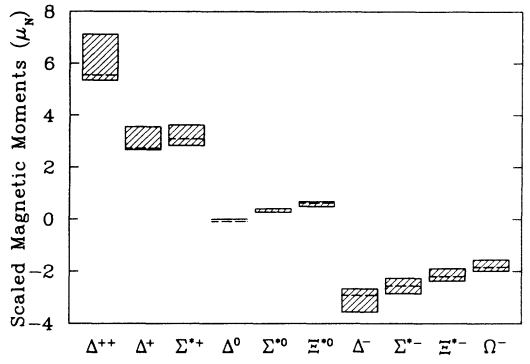

FIG. 14. Ratios of the lattice baryon magnetic moments to the lattice proton result scaled to reproduce the proton magnetic moment. Horizontal dashed lines indicate the simple quark model predictions.

TABLE VI. Neutral baryon rms charge radii in units of the proton radius $\langle\, |r^2/r_p^2|\, \rangle^{1/2}$.

Baryon	Radius
n	0.34(22)
Λ^0	0.39(8)
Σ^0	0.44(4)
Ξ^0	0.53(10)
Σ^{*0}	0.39(4)
Ξ^{*0}	0.57(9)

for the magnetic moment of the proton, where $A = 4/3$ and $B = 1/3$. The effective moment of the lattice u quark in the proton is defined by equating the lattice u-quark sector contribution to $\frac{4}{3}\mu_u$, the corresponding u-quark sector contribution of the simple quark model. Similarly, the lattice d-quark sector contribution is equated with $-\frac{1}{3}\mu_d$ in defining the effective d-quark moment. In Δ^+ the lattice u-quark sector is equated with $2\mu_u$ and the d-quark sector equals the effective d-quark moment. Numerical values for effective quark moments are summarized in Table X for both octet and decuplet baryons.

Approximate baryon independence of decuplet baryon effective quark moments is displayed in Fig. 15. Closer examination of effective u-quark magnetic moment ratios does reveal some small baryon dependence of the quark moments. These results are summarized in Table XI. The quenching of effective quark moments in hyperons is largely due to the baryon mass setting the scale at which quarks contribute to the baryon moment [42]. These results are in sharp contrast to the enormous baryon dependence of the effective quark moments seen in octet baryons as illustrated in Fig. 16.

It is instructive to consider ratios of the octet baryon effective quark moments with their decuplet partners. These ratios are illustrated in Fig. 17. In the simple quark model all of these ratios are equal to 1. Dramatic effects are seen for the singly represented quarks u_n, s_Σ, and u_Ξ where deviations from SU(6)-octet wave functions are large in the lattice results. All quarks show a signifi-

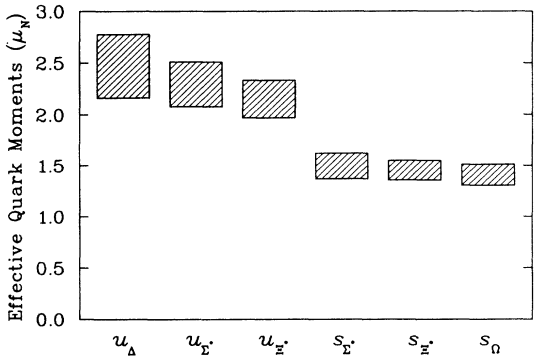

FIG. 15. Effective quark moments in decuplet baryons. Approximate baryon independence of the quark moments is displayed.

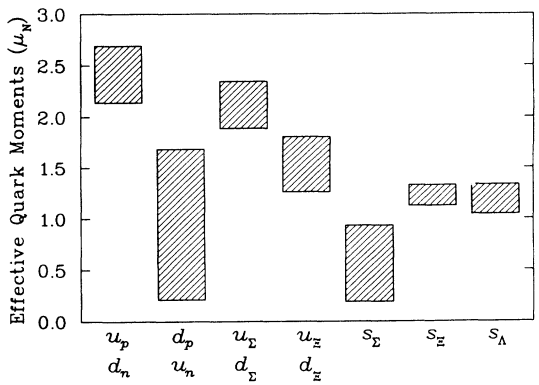

FIG. 16. Effective quark moments in octet baryons. Significant baryon dependence of the quark moments is illustrated.

TABLE VII. Baryon magnetic-dipole ($M1$) form factors in units of natural magnetons ($\mu_B = e/2M_B$).

Baryon	$\kappa_1 = 0.152$	$\kappa_2 = 0.154$	$\kappa_3 = 0.156$	$\kappa_{cr} = 0.1598(2)$
Δ^{++}	4.48(30)	4.48(42)	4.45(60)	4.44(87)
Δ^{+}	2.24(15)	2.24(21)	2.22(30)	2.22(44)
Δ^{0}	0.00	0.00	0.00	0.00
Δ^{-}	−2.24(15)	−2.24(21)	−2.22(30)	−2.22(44)
Σ^{*+}	2.24(15)	2.36(21)	2.47(30)	2.69(44)
Σ^{*0}	0.00	0.058(13)	0.119(45)	0.224(75)
Σ^{*-}	−2.24(15)	−2.25(19)	−2.24(24)	−2.24(32)
Ξ^{*0}	0.00	0.119(23)	0.235(68)	0.45(12)
Ξ^{*-}	−2.24(15)	−2.25(17)	−2.24(19)	−2.24(23)
Ω^{-}	−2.24(15)			−2.24(15)

cant baryon dependence with the exception of u_p/u_Δ and possibly u_Σ/u_{Σ^*}. This rich octet/decuplet baryon dependence in the effective quark moments contrasts that of the quark charge distribution radii as illustrated in the ratios of Fig. 11.

While lattice octet baryon moments differ significantly from the predictions of SU(6), it was not possible to determine how each of the coefficients $A = 4/3$ and $B = 1/3$ of (3.5) are altered. Using ratios of the u- and d-quark sector contributions to p or n and isospin symmetry, the octet baryon analysis indicates

$$\frac{B}{A} = 0.13^{+0.05}_{-0.11} < \frac{1}{4}, \tag{3.6}$$

where 1/4 is the SU(6) prediction. The decuplet baryon results indicate the effective moments and charge radii of doubly represented quarks are largely unchanged, suggesting $A \simeq 4/3$ and indicating B is better approximated by 1/6 than the standard SU(6) value of 1/3.

Considerable effort has gone into model calculations of the Δ^{++} and Ω^{-} magnetic moments. Here we collect together a handful of these calculations for comparison with our lattice results. Figure 18 displays ratios of Δ^{++}/p magnetic moments. The model calculations include results from the simple quark model [33] (QM), cloudy bag [43] (CB), Skyrme [44] (Skyr), Bethe-Salpeter [45] (BS), and QCD sum rule [46] (SR) analyses. The experimental (Expt) result is from a recent pion bremsstrahlung analysis [47] and therefore has some model dependence. Earlier papers reported larger values [48, 49] in better agreement with our lattice result.

Figure 19 displays ratios of Ω^{-}/p magnetic moments. The labels are as in Fig. 18 with additions of an additive quark model [50] in which effective masses (EM) of the quarks are used to estimate the intrinsic quark moments and a calculation in which relativistic corrections (RC) to baryon magnetic moments are considered [51]. Experimental (Expt) results are from a recent investigation where Ω^{-} hyperons are produced by a polarized neutral beam spin transfer reaction [52].

In the simple quark model the ratio of Ω^{-}/Λ^{0} magnetic moments is 3. The lattice results suggest that spin-dependent forces give rise to a larger strange quark moment in Ω^{-} relative to that in Λ^{0} as indicated in Fig. 17. The lattice ratio of Ω^{-}/Λ^{0} magnetic moments is $3.6^{+1.0}_{-0.6}$ suggesting an enhancement over the simple quark model ratio.

To complete the discussion of decuplet baryon magnetic-dipole properties Fig. 20 summarizes our calculation of magnetic radii normalized by the magnetic moment as in $\sqrt{\langle r^2\rangle/\mathcal{G}_{M1}(0)}$ (see Table XII). The magnetic radii follow a similar pattern to that of the charge radii.

E. Electric-quadrupole form factors

The results of the higher-order multipole moments must be regarded as preliminary due to the lack of symmetry in the spatial dimensions of our lattice. The elongated x dimension coupled with possible finite volume restrictions may induce deformations from spherical symmetry. On the other hand, it is useful to examine these quantities with a view toward determining the feasibility of extracting $E2$ moments in future calculations.

TABLE VIII. Magnetic-dipole ($M1$) form factors for single quarks of unit charge in units of natural magnetons ($\mu_B = e/2M_B$).

Quark	$\kappa_1 = 0.152$	$\kappa_2 = 0.154$	$\kappa_3 = 0.156$	$\kappa_{cr} = 0.1598(2)$
u_Δ	2.24(15)	2.24(21)	2.22(30)	2.22(44)
u_{Σ^*}	2.24(15)	2.30(20)	2.36(27)	2.46(38)
s_{Σ^*}	2.24(15)	2.13(17)	2.00(20)	1.79(25)
u_{Ξ^*}	2.24(15)	2.36(19)	2.48(24)	2.69(32)
s_{Ξ^*}	2.24(15)	2.19(16)	2.12(17)	2.02(19)
s_Ω	2.24(15)			2.24(15)

TABLE IX. Lattice results for decuplet baryon magnetic moments in units of nuclear magnetons (μ_N), ratios of decuplet baryon moments to the proton magnetic moment and ratios scaled to reproduce the proton magnetic moment.

Baryon	Magnetic moment (μ_N)	Ratio (μ/μ_p)	Scaled (μ_N)
Δ^{++}	4.91(61)	2.18(32)	6.09(88)
Δ^{+}	2.46(31)	1.09(16)	3.05(44)
Δ^{0}	0.00	0.00	0.00
Δ^{-}	−2.46(31)	−1.09(16)	−3.05(44)
Σ^{*+}	2.55(26)	1.13(14)	3.16(40)
Σ^{*0}	0.27(5)	0.118(24)	0.329(67)
Σ^{*-}	−2.02(18)	−0.90(10)	−2.50(29)
Ξ^{*0}	0.46(7)	0.206(35)	0.58(10)
Ξ^{*-}	−1.68(12)	−0.744(85)	−2.08(24)
Ω^{-}	−1.40(10)	−0.621(78)	−1.73(22)

The $E2$ form factor is particularly interesting since it provides a glimpse into the shape of the baryon ground state. A small $E2$ form factor would cast serious doubt on Skyrme models where the hedgehog Skyrmion has an inherently large quadrupole moment. Our focus here is on estimating an upper bound for the $E2$ form factor. Tables XIII and XIV summarize the lattice results for $E2$ form factors.

The negative sign of the central values for positively charged baryons is consistent with the deformation one might expect from our elongated lattice. Equation (2.23b) isolates the spin matrix element

$$\left\langle \frac{3}{2}s' \mid \Sigma_0^{(2)} \mid \frac{3}{2}s \right\rangle$$

and therefore determines the asymmetry of the ground-state wave function having some overlap with the spherical harmonic $Y_{20}(\theta)$ where θ is measured relative to the spin quantization axis $\hat{z}$. A negative $E2$ moment corresponds to an oblate shape which may be due to some broadening of the wave function in the longer x direction where overlap with periodic images is minimized.

In nonrelativistic models where angular momentum l and spin s are constants of the motion, it is useful to consider angular momentum selection rules. Consider the transition

$$\left\langle j' = l' + s' \mid j_\gamma \mid j = l + s \right\rangle, \tag{3.7}$$

TABLE X. Effective quark magnetic moments for quarks of unit charge in units of nuclear magnetons (μ_N).

Octet baryons		Decuplet baryons	
Quark	Effective moment	Quark	Effective moment
u_p	2.41(27)	u_Δ	2.46(31)
d_p	1.10(74)	d_Δ	2.46(31)
u_Σ	2.12(23)	u_{Σ^*}	2.29(22)
s_Σ	0.59(37)	s_{Σ^*}	1.49(13)
u_Ξ	1.53(27)	u_{Ξ^*}	2.14(18)
s_Ξ	1.24(10)	s_{Ξ^*}	1.45(10)
s_Λ	1.25(15)	s_Ω	1.40(10)

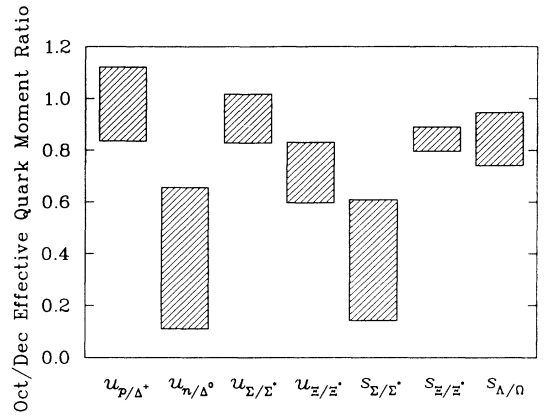

FIG. 17. Ratios of octet baryon effective quark moments with their decuplet partners. Octet/decuplet dependence is seen throughout the quarks with the exception of u_p/u_Δ and possibly u_Σ/u_{Σ^*}.

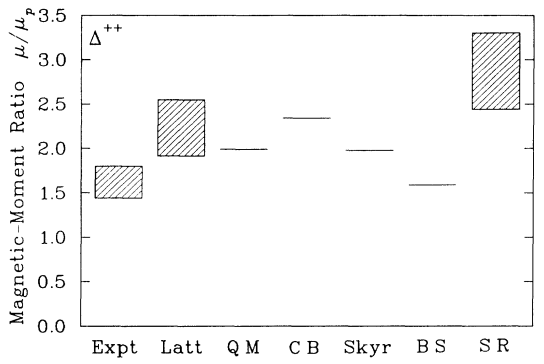

FIG. 18. Comparison of the lattice Δ^{++}/p magnetic moment ratio (Latt) with model calculations and an experimental result (Expt) having some model dependence. The model calculations are the simple quark model (QM), cloudy bag (CB), Skyrme (Skyr), Bethe-Salpeter (BS), and QCD sum rules (SR). References are given in the text.

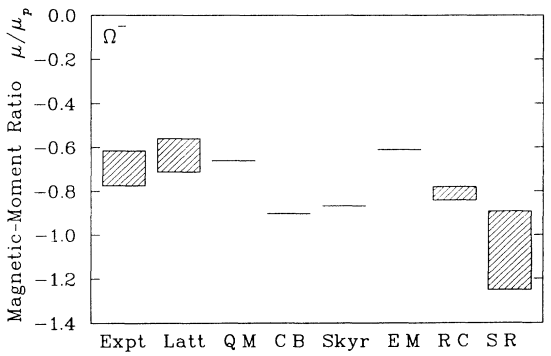

FIG. 19. Comparison of the lattice Ω^-/p magnetic moment ratio (Latt) with model calculations and experiment (Expt). The model calculations are as in Fig. 18 with additions of an additive quark model based on effective quark masses (EM) and a calculation including relativistic corrections (RC). References are given in the text.

where j_γ is the total angular momentum of the photon and determines the multipole character of the transition. Total angular momentum selection rules require $j + j_\gamma = j'$ and therefore

$$|j - j'| \le j_\gamma \le j + j'. \tag{3.8}$$

Combined with parity conservation, (3.8) indicates there are at most four multipole form factors available in spin-3/2 to spin-3/2 transitions. Electric form factors correspond to $s = s'$. This yields the orbital angular momentum selection rule

$$|l - l'| \le j_\gamma \le l + l', \tag{3.9}$$

indicating the $E2$ form factor vanishes in nonrelativistic models unless some configuration mixing is included in the baryon ground state.

The relationship between our definition of the $E2$ form factor given in (2.16a) and that usually calculated in models may be easily established by writing (2.16a) using the spherical harmonics in the Breit frame with $s = s' = j = 3/2$. Noting that

$$[\hat{q} \times \hat{q}]^{(2)}_m = \sqrt{\frac{8\pi}{15}}\, Y_{2m}(\hat{q}), \tag{3.10}$$

Eq. (2.16a) may be written as

$$\left\langle \frac{\mathbf{q}}{2}, \frac{3}{2} \,\middle|\, j^0(0) \,\middle|\, -\frac{\mathbf{q}}{2}, \frac{3}{2} \right\rangle = G_{E0}(q^2) + \frac{2}{3}\tau \sqrt{\frac{4\pi}{5}}\, Y_{20}(\hat{q})\, G_{E2}(q^2). \tag{3.11}$$

Model approaches determine current matrix elements via the Fourier transform

$$\left\langle \frac{\mathbf{q}}{2}, \frac{3}{2} \,\middle|\, j^0(0) \,\middle|\, -\frac{\mathbf{q}}{2}, \frac{3}{2} \right\rangle = \int d^3r\, e^{i\mathbf{q}\cdot\mathbf{r}}\, \overline{\psi}(r)\, j^0(r)\, \psi(r). \tag{3.12}$$

Using the small $|\mathbf{q}|$ spherical harmonic expansion

$$e^{i\mathbf{q}\cdot\mathbf{r}} = 4\pi \sum_{l=0}^{\infty} \frac{i^l}{(2l+1)!!}\, q^l r^l \sum_{m=-l}^{l} Y^*_{lm}(\hat{r})\, Y_{lm}(\hat{q}), \tag{3.13}$$

and choosing $\mathbf{q} = q\hat{z}$, it is straightforward to show

$$\mathcal{G}_{E2}(0) = M_B^2 \int d^3r\, \overline{\psi}(r)\, (3z^2 - r^2)\, \psi(r), \tag{3.14}$$

where $3z^2 - r^2$ is the standard operator used for quadrupole moments. The factor M_B^2 indicates that $\mathcal{G}_{E2}(0)$ gives the $E2$ form factor in units of (e/M_B^2).

A chiral quark model calculation [53] gives $\mathcal{G}_{E2}(0) = -0.30$ fm^2 for Δ^{++} which lies 2σ outside our bound of $-0.03(13)$ fm^2. However it may be more appropriate to compare the dimensionless ratio of the $E2$ form factor and the squared charge radius. The generic Skyrme model result is [53, 54]

$$\frac{\mathcal{G}_{E2}}{\langle r^2 \rangle_V} = -\frac{4}{25} I_3, \tag{3.15}$$

where $\langle r^2 \rangle_V$ is the isovector charge radius and I_3 is the 3-component of isospin. The analogous lattice ratio is

$$\frac{\mathcal{G}_{E2}}{\langle r^2 \rangle_V} = \left(I_3 + \frac{1}{2}\right) \frac{\mathcal{G}^{\Delta^+}_{E2}}{\langle r^2 \rangle^{\Delta^+}}. \tag{3.16}$$

The isospin dependence of the lattice results is proportional to the baryon charge which is not the case for the Skyrme model. For Δ^{++} the lattice ratio is $-0.08(30)$ which encompasses the Skyrme model ratio of -0.24. Future high statistics lattice calculations on a cubic lattice should be able to confirm or reject the hedgehog Skyrmion description of baryons.

TABLE XI. Effective u- and s-quark magnetic moment ratios.

Quark ratio	Lattice result
u_{Σ^*}/u_Δ	0.93(5)
u_{Ξ^*}/u_{Σ^*}	0.94(3)
u_{Ξ^*}/u_Δ	0.87(7)
s_{Ξ^*}/s_{Σ^*}	0.97(5)
s_Ω/s_{Ξ^*}	0.97(3)
s_Ω/s_{Σ^*}	0.94(7)

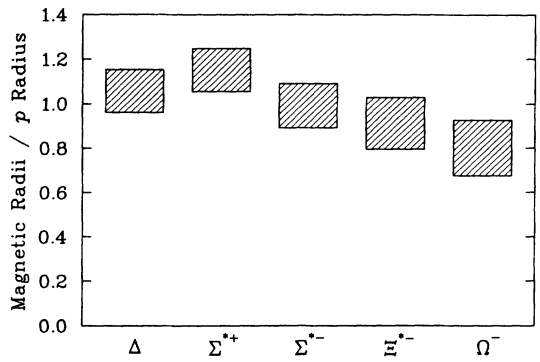

FIG. 20. Magnetic radii of decuplet baryons in units of the proton magnetic radius. The magnetic radii follow a similar pattern to that of the charge radii.

F. Magnetic-octupole form factors

The magnetic-octupole form factors are large for heavy quark masses and appear to decrease as the quark mass becomes lighter. In the physical regime the uncertainties

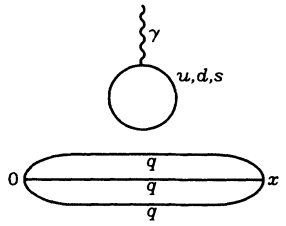

FIG. 21. A skeleton diagram of a disconnected quark loop contributing to the magnetic moment of a baryon. The diagram may be dressed with an arbitrary number of gluons.

TABLE XII. Baryon magnetic radii $\sqrt{\langle r^2 \rangle / (\mathcal{G}_{M1} a^2)}$ in lattice units.

Baryon	$\kappa_1 = 0.152$	$\kappa_2 = 0.154$	$\kappa_3 = 0.156$	$\kappa_{cr} = 0.1598(2)$
Δ^{++}	3.71(13)	4.02(19)	4.34(39)	4.90(57)
Δ^{+}	3.71(13)	4.02(19)	4.34(39)	4.90(57)
Δ^{-}	3.71(13)	4.02(19)	4.34(39)	4.90(57)
Σ^{*+}	3.71(13)	4.13(19)	4.58(38)	5.34(56)
Σ^{*-}	3.71(13)	3.93(17)	4.19(29)	4.59(41)
Ξ^{*-}	3.71(13)	3.82(14)	3.98(18)	4.22(23)
Ω^{-}	3.71(13)			3.71(13)

TABLE XIII. Baryon electric-quadrupole ($E2$) form factors in units of (e/M_B^2).

Baryon	$\kappa_1 = 0.152$	$\kappa_2 = 0.154$	$\kappa_3 = 0.156$	$\kappa_{cr} = 0.1598(2)$
Δ^{++}	−0.6(8)	−0.8(14)	−0.7(28)	−1.0(39)
Δ^{+}	−0.3(4)	−0.4(7)	−0.4(14)	−0.5(19)
Δ^{0}	0.0	0.0	0.0	0.0
Δ^{-}	0.3(4)	0.4(7)	0.4(14)	0.5(19)
Σ^{*+}	−0.3(4)	−0.3(7)	−0.1(13)	−0.1(19)
Σ^{*0}	0.00	0.05(7)	0.15(23)	0.26(36)
Σ^{*-}	0.3(4)	0.4(6)	0.4(9)	0.5(13)
Ξ^{*0}	0.00	0.07(12)	0.15(31)	0.29(54)
Ξ^{*-}	0.3(4)	0.3(5)	0.4(6)	0.4(8)
Ω^{-}	0.3(4)			0.3(4)

TABLE XIV. Electric-quadrupole ($E2$) form factors for single quarks of unit charge in units of (e/M_B^2).

Quark	$\kappa_1 = 0.152$	$\kappa_2 = 0.154$	$\kappa_3 = 0.156$	$\kappa_{cr} = 0.1598(2)$
u_Δ	−0.3(4)	−0.4(7)	−0.4(14)	−0.5(19)
u_{Σ^*}	−0.3(4)	−0.3(6)	−0.3(11)	−0.3(16)
s_{Σ^*}	−0.3(4)	−0.4(5)	−0.7(6)	−1.0(8)
u_{Ξ^*}	−0.3(4)	−0.3(6)	−0.2(9)	−0.2(12)
s_{Ξ^*}	−0.3(4)	−0.4(4)	−0.5(5)	−0.6(6)
s_Ω	−0.3(4)			−0.3(4)

TABLE XV. Baryon magnetic-octupole ($M3$) form factors in units of $(e/2M_B^3)$.

Baryon	$\kappa_1 = 0.152$	$\kappa_2 = 0.154$	$\kappa_3 = 0.156$	$\kappa_{cr} = 0.1598(2)$
Δ^{++}	113±30	99±51	80±73	55±112
Δ^{+}	56±15	50±25	40±37	27±56
Δ^{0}	0±0	0±0	0±0	0±0
Δ^{-}	−56±15	−50±25	−40±37	−27±56
Σ^{*+}	56±15	54±27	48±48	43±72
Σ^{*0}	0±0	0.8±2.9	−0.4±7.7	0.3±1.4
Σ^{*-}	−56±15	−52±22	−49±34	−41±49
Ξ^{*0}	0±0	2±5	2±14	6±24
Ξ^{*-}	−56±15	−54±19	−54±25	−51±32
Ω^{-}	−56±15	−56±15	−56±15	−56±15

TABLE XVI. Magnetic-octupole ($M3$) form factors for single quarks of unit charge in units of $(e/2M_B^3)$.

Quark	$\kappa_1 = 0.152$	$\kappa_2 = 0.154$	$\kappa_3 = 0.156$	$\kappa_{cr} = 0.1598(2)$
u_Δ	56±15	50±25	40±37	27±56
u_{Σ^*}	56±15	53±24	48±41	42±61
s_{Σ^*}	56±15	51±17	49±22	41±28
u_{Ξ^*}	56±15	57±23	56±37	57±55
s_{Ξ^*}	56±15	53±16	52±19	48±22
s_Ω	56±15	56±15	56±15	56±15

are sufficiently large to make the $M3$ moments consistent with zero with the exceptions of Ξ^{*-} and Ω^- hyperons. Tables XV and XVI summarize the lattice results for decuplet baryons and their quark contributions respectively.

Angular momentum selection rules for $M3$ moments require $s + 1 = s'$ limiting nonvanishing transitions to

$$||l - l'| - 1| \leq j_\gamma \leq l + l' + 1. \tag{3.17}$$

Once again $M3$ transitions require nonzero orbital angular momentum admixtures in the ground-state wave function. Connection to model calculations of $M3$ moments may be made from our definition of the $M3$ moment in (2.16b) in a manner analogous to that for the $E2$ moment. $M3$ moments in hedgehog models [53] are $1/N_c$ suppressed relative to $M1$ moments and cannot be determined using conventional semiclassical methods.

The dimensionless ratio of interest for $M3$ moments relates the $M3$ form factor to the $M1$ form factor and the squared charge radius. For Ω^- the ratio is

$$\frac{\mathcal{G}_{M3}}{\mathcal{G}_{M1} \langle r^2 \rangle} = 1.4(4), \tag{3.18}$$

indicating a relatively large $M3$ moment. This ratio is much larger than one might expect from our discussion of the $E2$ form factor and angular momentum selection rules. For Ω^- the ratio is

$$\frac{\mathcal{G}_{E2}}{\langle r^2 \rangle} = 0.02(3). \tag{3.19}$$

However, in fully relativistic calculations angular momentum and spin on their own are no longer good quantum numbers. Gluons may also carry angular momentum allowing radical changes from standard SU(6)-spin-flavor symmetry as seen in the magnetic properties of octet baryons and evidenced in the European Muon Collaboration (EMC) polarized muon-proton scattering experiment [55]. Furthermore, lattice QCD is a relativistic theory with particle creation and annihilation allowing some overlap with mesonic dressings of baryons even in the quenched approximation.

This pattern of small electric effects and large magnetic effects is reminiscent of the electromagnetic properties of octet baryons. The lattice results show a spin dependence in the quark distributions that accounts for the negative squared charge radius of the neutron by *slightly* increasing the d-quark distribution radius relative to the u-quark radius. However, spin dependence in the magnetic properties is huge. For example, Fig. 16 shows that the effective magnetic moment of a u quark in the neutron is roughly half that of the d quark when normalized to unit charge.

IV. OVERVIEW AND OUTLOOK

We have presented a fully relativistic formalism for isolating and extracting the four electromagnetic multipole form factors of spin-3/2 systems in lattice field theory. Results of the first lattice QCD analysis of SU(3)-flavor decuplet baryons have been systematically examined to reveal new aspects of the underlying nonperturbative quark-gluon dynamics.

The $E0$ and $M1$ correlation functions for decuplet baryons show a broad plateau region allowing a reliable extraction of the electromagnetic form factors. Statistical uncertainties are similar to that seen in our octet baryon analysis.

The qualitative mass dependence of decuplet baryon charge radii follows the anticipated pattern produced by a more localized strange quark distribution. The electric form factors of neutral baryons are dominated by the net charge of the light quarks as in the octet-baryon results. Model calculations of the Ω^- charge radius vary widely and the lattice results favor a calculation based on a relativized quark model [37] over the other bag and Skyrme models considered.

Closer examination of the baryon charge radii reveals a behavior in the quark charge distribution radii consistent with a spin-dependent force having an inverse relationship with the quark mass. This behavior is what one expects from the hyperfine interaction term of the one-gluon-exchange potential. The spin-dependent force counteracts center-of-mass shifts and suppresses baryon dependence of the quark charge distribution radii.

The center-of-mass shifts that give rise to an enhancement of the u-quark magnetic moment in the octet Ξ^0 relative to that in the neutron are offset by this repulsive force in decuplet baryons. Variation in the quark effective magnetic moments from baryon to baryon is minimal for decuplet baryons. The residual effect is largely due to the baryon mass setting the scale at which quarks contribute to the baryon magnetic moment.

The symmetric role of quarks in decuplet baryons contrasts that in octet baryons. The role of a quark in an octet baryon correlation function is different depending

on whether the quark is singly or doubly represented. This difference, which cannot arise in the decuplet case, causes large variations in the electromagnetic properties of quarks in octet baryons.

The lattice predictions of decuplet baryon magnetic moments agree with the simplest of quark models to a remarkable extent. This is in sharp contrast to the octet baryon analysis and is due to an approximate baryon independence of effective quark magnetic moments in decuplet baryons. The lattice prediction of the Δ^{++}/p magnetic moment ratio is large compared to a recent experimental analysis [47] but compares better with previous analyses. Our Ω^- magnetic moment agrees with experiment [52] and prefers the simple quark model result and a calculation based on effective quark masses [50] over the other four model calculations considered.

The $E2$ and $M3$ form factors depend on subtle differences in the correlation function ratios and as a result have larger statistical uncertainties. The $M3$ form factors are finite at all the values of κ considered. The $E2$ form factor is at the threshold of confirming or rejecting the hedgehog Skyrmion description of baryons. A future high statistics lattice calculation on a cubic lattice will provide considerable insight.

For electromagnetic form factors to provide a reliable test of QCD, one must understand and eliminate systematic errors. While the results of chiral perturbation theory may be used to assess the magnitude of possible systematic errors in the lattice extrapolation procedure [35], there can be no substitute to actual calculations probing regimes of lighter quark mass.

A calculation of electromagnetic properties in full QCD would also assist in understanding systematic errors. However, to calculate in full QCD, the contributions of disconnected quark loops as illustrated in Fig. 21 must also be understood. These loop contributions may play a key role in removing the discrepancies between lattice and experimental violations of magnetic moment sum rules [42]. Closed quark loop contributions may be estimated even in the quenched approximation and present a major challenge for future lattice QCD calculations. Such a calculation will provide insight into important questions such as the strangeness content of the proton and the general role played by sea quarks in hadrons.

The examination of decuplet baryon structure through the lattice field theory approach to QCD has given a new and more detailed understanding of nonperturbative interactions. The underlying theme of the results presented here involves a cancellation of spin-dependent forces and center-of-mass effects, which results in a structure that is consistent with nondynamical models such as the simplest quark model based on SU(6)-spin-flavor symmetry broken only by the quark masses.

A future investigation [14] will address $N\gamma \to \Delta$ transitions where there have been significant experimental effort to measure the $M1$ and $E2$ transition moments. This, of course, has been accompanied by a plethora of model calculations for these quantities. The lattice results will be instrumental in assessing the reliability of the model analyses.

The odd-parity spin-3/2 baryon octet also offers an interesting forum for checking model predictions. There has not been a lattice investigation of these states. The $N(1520)$ is the lowest-lying baryon with $I(J^P) = \frac{1}{2}(\frac{3}{2}^-)$. It is expected to be stable with our present lattice parameters and therefore is accessible to lattice calculations. The neighboring $N\frac{1}{2}^-(1535)$ is a source of possible contamination in the $j = 3/2$ interpolating field, and therefore angular momentum projection operators may be required [56]. Calculations of the electromagnetic properties of $N\frac{3}{2}^-(1520)$ may be completely different from model expectations if gluons carry a significant fraction of the angular momentum usually attributed to quark degrees of freedom alone. With the anticipated experimental program at the Continuous Electron Beam Accelerator Facility (CEBAF), a lattice QCD analysis of $N\frac{1}{2}^+\gamma \to N\frac{3}{2}^-$ transition moments is also of interest.

It is very encouraging that lattice QCD evaluations of hadronic electromagnetic form factors give, for example, a pattern of magnetic moments which is as good or better than hadronic models with adjustable parameters, which in some cases have been tuned to fit magnetic moments. With further study to understand and eliminate systematic errors, we believe the study of hadron electromagnetic form factors will prove ultimately to be one of the best quantitative testing grounds for nonperturbative QCD.

ACKNOWLEDGMENTS

The computing resources for this study were provided by the Computing Science Department and the Center for Computational Sciences at the University of Kentucky on their IBM 3090-600J supercomputer. D.B.L. thanks Thomas Cohen, Wojciech Broniowski, and Manoj Banerjee for enthusiastic discussions. T.D. thanks Keh-Fei Liu for many useful conversations. This work was supported in part by the U.S. Department of Energy under Grant Nos. DE-FG05-87ER-40322 and DE-FG05-84ER-40154, the National Science Foundation under Grant No. STI-9108764 and the Natural Sciences and Engineering Research Council of Canada.

[1] D. B. Leinweber, R. M. Woloshyn, and T. Draper, Phys. Rev. D **43**, 1659 (1991).
[2] T. Draper, R. M. Woloshyn, and K. F. Liu, Phys. Lett. B **234**, 121 (1990).
[3] W. Wilcox and R. M. Woloshyn, Phys. Rev. Lett. **54**, 2653 (1985).
[4] R. M. Woloshyn and A. M. Kobos, Phys. Rev. D **33**, 222 (1986).
[5] R. M. Woloshyn, Phys. Rev. D **34**, 605 (1986).
[6] T. Draper, R. M. Woloshyn, W. Wilcox, and K. F. Liu,

in *Field Theory on the Lattice*, Proceedings of the International Symposium, Seillac, France, 1987, edited by A. Billoire *et al.* [Nucl. Phys. B (Proc. Suppl.) **4**, 524 (1988)].
[7] G. Martinelli and C. T. Sachrajda, Nucl. Phys. **B306**, 865 (1988).
[8] T. Draper, R. M. Woloshyn, W. Wilcox, and K. F. Liu, Nucl. Phys. **B318**, 319 (1989).
[9] G. Martinelli and C. T. Sachrajda, Nucl. Phys. **B316**, 355 (1989).
[10] W. Wilcox, T. Draper, and K. F. Liu, Phys. Rev. D **46**, 1109 (1992).
[11] W. Wilcox and K. F. Liu, Phys. Lett. B **172**, 62 (1986).
[12] W. Wilcox, Phys. Rev. D **43**, 2443 (1991).
[13] M. C. Chu, M. Lissia, and J. W. Negele, Nucl. Phys. **B360**, 31 (1991).
[14] D. B. Leinweber, T. Draper, and R. M. Woloshyn (unpublished).
[15] S. Nozawa and D. B. Leinweber, Phys. Rev. D **42**, 3567 (1990).
[16] B. L. Ioffe, Nucl. Phys. **B188**, 317 (1981).
[17] Y. Chung, H. G. Dosch, M. Kremer, and D. Schall, Nucl. Phys. **B197**, 55 (1982).
[18] J. Sakurai, *Advanced Quantum Mechanics* (Addison-Wesley, Reading, MA, 1967).
[19] C. Itzykson and J. Zuber, *Quantum Field Theory* (McGraw-Hill, New York, 1980).
[20] W. Rarita and J. Schwinger, Phys. Rev. **60**, 61 (1941).
[21] M. Benmerrouche, R. M. Davidson, and N. C. Mukhopadhyay, Phys. Rev. C **39**, 2339 (1989).
[22] V. M. Belyaev and B. L. Ioffe, Zh. Eksp. Teor. Fiz. [Sov. Phys. JETP **57**, 716 (1983)].
[23] A. R. Edmonds, *Angular Momentum in Quantum Mechanics* (Princeton University Press, Princeton, NJ, 1960).
[24] J. G. Körner and M. Kuroda, Phys. Rev. D **16**, 2165 (1977).
[25] C. Bernard, T. Draper, G. Hockney, and A. Soni, in *Lattice Gauge Theory: A Challenge in Large-Scale Computing*, Proceedings of the NATO Advanced Study Institute, Wuppertal, West Germany, 1985, edited by B. Bunk, K. H. Mutter, and K. Schilling, NATO ASI Series B: Physics Vol. 140 (Plenum, New York, 1986).
[26] C. Bernard, in *Gauge Theory on a Lattice*, edited by C. Zachos, W. Celmaster, E. Kovacs, and D. Sivers (National Technical Information Service, Springfield, 1984).
[27] T. Draper, Ph.D. thesis, UCLA, 1984.
[28] T. Draper, R. M. Woloshyn, W. Wilcox, and K. F. Liu, in *Lattice '88*, Proceedings of the International Symposium, Batavia, Illinois, 1988, edited by A. S. Kronfeld and P. B. MacKenzie [Nucl. Phys. B (Proc. Suppl.) **9** (1989)].
[29] N. Cabibbo and E. Marinari, Phys. Rev. Lett. **119B**, 387 (1982).
[30] This proved sufficient to achieve good statistical independence of the ensemble. An examination of a number of observables, configuration by configuration, revealed no apparent long-range correlation in our gauge configuration sample.
[31] B. Efron, SIAM Rev. **21**, 460 (1979).
[32] S. Gottlieb, P. B. MacKenzie, H. B. Thacker, and D. Weingarten, Nucl. Phys. **B263**, 704 (1986).
[33] Particle Data Group, J. J. Hernández *et al.*, Phys. Lett. B **239**, 1 (1990).
[34] M. A. B. Bég and A. Zepeda, Phys. Rev. D **6**, 2912 (1972).
[35] D. B. Leinweber and T. D. Cohen, University of Maryland Report No. 92-190 (unpublished).
[36] While there is some overlap in the error bars of Fig. 7, a calculation of the change of the strange quark distribution radius indicates the radius is strictly decreasing as the u quarks become lighter. This is not the case for the decuplet Σ^{*+}.
[37] N. Barik, S. N. Jena, and D. P. Rath, Phys. Rev. D **41**, 1568 (1990).
[38] J. Kunz, P. J. Mulders, and G. A. Miller, Phys. Lett. B **255**, 11 (1991).
[39] J. Kunz and P. J. Mulders, Phys. Rev. D **41**, 1578 (1990).
[40] G. Höhler *et al.*, Nucl. Phys. **B114**, 505 (1976).
[41] O. Dumbrajs, Nucl. Phys. **B216**, 277 (1983).
[42] D. B. Leinweber, Phys. Rev. D **45**, 252 (1992).
[43] M. I. Krivoruchenko, Yad. Fiz. **45**, 169 (1987) [Sov. J. Nucl. Phys. **45**, 109 (1987)].
[44] J. H. Kim, C. H. Lee, and H. K. Lee, Nucl. Phys. **A501**, 835 (1989).
[45] A. Mitra and A. Mittal, Phys. Rev. D **29**, 1399 (1984).
[46] V. M. Belyaev, ITEP report, 1992 (unpublished).
[47] A. Bosshard *et al.*, Phys. Rev. D **44**, 1962 (1991).
[48] B. M. K. Nefkens *et al.*, Phys. Rev. D **18**, 391 (1978).
[49] R. Wittman, Phys. Rev. D **37**, 2075 (1988).
[50] K. T. Chao, Phys. Rev. D **41**, 920 (1990).
[51] H. Georgi and A. Manohar, Phys. Lett. **132B**, 183 (1983).
[52] H. T. Diehl *et al.*, Phys. Rev. Lett. **67**, 804 (1991).
[53] T. D. Cohen and W. Broniowski, Phys. Rev. D **34**, 3472 (1986); and (private communication).
[54] G. S. Adkins, C. R. Nappi, and E. Witten, Nucl. Phys. **B228**, 552 (1983).
[55] European Muon Collaboration, J. Ashman *et al.*, Phys. Lett. B **206**, 364 (1988); Nucl. Phys. **B238**, 1 (1989).
[56] D. B. Leinweber, Ann. Phys. (N.Y.) **198**, 203 (1990).